ISSN: (Print) (Online) Journal homepage: <https://www.tandfonline.com/loi/tbsd20>

Design, synthesis, and computational studies of benzimidazole derivatives as new antitubercular agents

Gozde Yalcin-Ozkat, Ronak H. Ersan, Mahmut Ulger, Seda T. Ulger, Serdar Burmaoglu, Ilkay Yildiz & Oztekin Algul

To cite this article: Gozde Yalcin-Ozkat, Ronak H. Ersan, Mahmut Ulger, Seda T. Ulger, Serdar Burmaoglu, Ilkay Yildiz & Oztekin Algul (2022): Design, synthesis, and computational studies of benzimidazole derivatives as new antitubercular agents, Journal of Biomolecular Structure and Dynamics, DOI: [10.1080/07391102.2022.2036241](https://doi.org/10.1080/07391102.2022.2036241)

To link to this article: <https://doi.org/10.1080/07391102.2022.2036241>



View supplementary material [↗](#)



Published online: 08 Feb 2022.



Submit your article to this journal [↗](#)



Article views: 341







View related articles [↗](#)



View Crossmark data [↗](#)



Design, synthesis, and computational studies of benzimidazole derivatives as new antitubercular agents

Gozde Yalcin-Ozkat^{a,b} , Ronak H. Ersan^{c,d}, Mahmut Ulger^e, Seda T. Ulger^f, Serdar Burmaoglu^g , Ilkay Yildiz^h  and Oztekin Algul^c 

^aMax Planck Institute for Dynamics of Complex Technical Systems, Molecular Simulations and Design Group, Magdeburg, Germany; ^bFaculty of Engineering, Bioengineering Department, Recep Tayyip Erdogan University, Rize, Turkey; ^cDepartment of Pharmaceutical Chemistry, Faculty of Pharmacy, Mersin University, Mersin, Turkey; ^dDepartment of Medical Laboratory, Cihan University, Duhok, Iraq; ^eDepartment of Pharmaceutical Microbiology, Faculty of Pharmacy, Mersin University, Mersin, Turkey; ^fDepartment of Medical Microbiology, Faculty of Medicine, Mersin University, Mersin, Turkey; ^gDepartment of Chemistry, Faculty of Science, Ataturk University, Erzurum, Turkey; ^hDepartment of Pharmaceutical Chemistry, Faculty of Pharmacy, Ankara University, Ankara, Turkey

Communicated by Ramaswamy H. Sarma.

ABSTRACT

The increase in the drug-resistant strains of *Mycobacterium tuberculosis* has led researchers to new drug targets. The development of new compounds that have effective inhibitory properties with the selective vital structure of *Mycobacterium tuberculosis* is required in new scientific approaches. The most important of these approaches is the development of inhibitor molecules for Mycobacterium cell wall targets. In this study, first of all, the antitubercular activity of 23 benzimidazole derivatives was experimentally determined. And then molecular docking studies were carried out with 4 different targets: Arabinosyltransferase C (EmbC), Filamentous Temperature Sensitive Mutant Z (FtsZ), Protein Tyrosine Phosphatase B (PtpB), and Decaprenylphosphoryl- β -D-ribose-2'-oxidase (DprE1). It has been determined that benzimidazole derivatives show activity through the DprE1 enzyme. It is known that DprE1, which has an important role in the synthesis of the cell envelope from Arabinogalactan, is also effective in the formation of drug resistance. Due to this feature, the DprE1 enzyme has become an important target for drug development studies. Also, it was chosen as a target for this study. This study aims to identify molecules that inhibit DprE1 for the development of more potent and selective antitubercular drugs. For this purpose, molecular docking studies by AutoDock Vina, and CDOCKER and molecular dynamics (MD) simulations and *in silico* ADME/Tox analysis were implemented for 23 molecules. The molecules exhibited binding affinity values of less than -8.0 kcal/mol. After determining the compound's anti-TB activities by a screening test, the best-docked results were detected using compounds **20**, **21**, and **30**. It was found that **21**, was the best molecule with its binding affinity value, which was supported by MD simulations and *in silico* ADME modeling results.

ARTICLE HISTORY

Received 12 August 2021
Accepted 26 January 2022

KEYWORDS

Benzimidazole; DprE1; molecular docking; molecular dynamics simulations; ADME

1. Introduction

One of the top 10 causes of death worldwide and the leading cause of death from a single infectious agent is tuberculosis (TB). It is caused by the bacillus *Mycobacterium tuberculosis* (MTB), which is spread when people with TB expel bacteria into the air. The current pace of change is not enough, according to a report from the World Health Organization; the global cumulative reduction rate for TB incidence was only 6.3% between 2015 and 2018, which is much less than that of the 2020 milestone of 20% (Harding, 2020; <https://www.who.int/publications/i/item/global-tuberculosis-report-2019>). Because of some reasons as multi-resistant strains of MTB, immigration from countries with high rates of TB infection, or the feature of changing between replicative and dormant states of MTB, re-emergence generates the biggest problem for TB (Riccardi et al., 2013). With this, the

importance of the design of the novel drug molecules, especially resistant strains, increases.

The key enzyme involved in the arabinogalactan biosynthesis is a component of the mycobacterium cell wall (Riccardi et al., 2013). Following the discovery of nitrobenzothiazinone, which binds covalently to the DprE1 enzyme, became a growing interest for this target (Makarov et al., 2009). Besides this, the development of new molecular structures has begun for TB treatment.

The development of novel antimycobacterial lead molecules is the focus of the ongoing study, mainly on computational studies on the DprE1 enzyme's active site as an essential aspect of MTB survival and as a novel mechanism of antitubercular activity. In addition, new molecular structures are being developed for treating TB.

Benzimidazole and its derivatives exhibit antibacterial, antifungal, antitubercular, antimalarial, anti-inflammatory, analgesic,

anti-amoebic, antiulcerative, antioxidant, antihypertensive, antiallergic, antiproliferative, antitumor, and anti-HIV-1 properties (Djemoui et al., 2020; Kopel et al., 2015). *In vitro* and *in silico* studies of their activities revealed that those benzimidazole derivatives as pyridobenzimidazole also abrogate MTB's bactericidal activity (Warrier et al., 2016). In addition, they have the potential to be anti-TB agents because of the simplicity and speed of their synthesis, along with other important features of benzimidazoles. Benzimidazole has always aroused researchers' interest, not only from a synthetic or biosynthetic point of view but also because of its interesting biological characteristics. For instance, 2-benzoxazolinone is a closely related bioisostere of some scaffolds such as benzoxazoles, benzimidazole, benzothiazolinone, and benzothiazoles, which showed strong interactions with the key amino acid residues in the active site of DprE1 (Stanley et al., 2012).

Considering these advantages, computational studies of benzimidazole derivatives with DprE1 enzyme inhibitors and antitubercular drug design were carried out in this study. These computational studies were performed using 23 molecules thought to inhibit the DprE1 enzyme. Substituted benzimidazole compounds were investigated in this study. This study is important to know the substituted benzimidazoles' effects.

2. Materials and methods

2.1. Synthesis of selected compounds

In this work, a set of 23 of non/di/tri-substituted benzimidazole and non or 5-substituted bisbenzimidazole derivatives, as shown in Table 1, were obtained from the published data (Akpa et al., 2016; Ayaz et al., 2020; Boggu et al., 2016; Duran et al., 2020; Ersan et al., 2020; 2021; Gozelle et al., 2019; Gümüs et al., 1989; Niknam & Fatehi-Raviz, 2007; Oren et al., 1997; Phillips, 1928; Wang et al., 2006). Among the selected compounds, **21** is the only newly synthesized compound. The synthesis method and characterization data for compound **21** are shown in the supporting information. The structures of all compounds were confirmed by infrared (IR), proton nuclear magnetic resonance (^1H NMR), and carbon-13 NMR (^{13}C NMR) spectroscopy.

2.2. Antitubercular activity

2.2.1. Agar proportion method

As recommended by the Clinical Laboratory Standards Institute (CLSI), the minimum inhibitory concentration (MIC) values of each synthesized compound were obtained by duplicate agar dilution (National Committee for Clinical Laboratory Standards, 2003; Clinical and Laboratory Standards Institute (CLSI) (formerly NCCLS), 2002). In each assay, positive and negative growth controls were used. Isoniazid (INH; Sigma I3377) and ethambutol (EMB; Sigma E4630) were used as control agents. Provided by Refik Saydam National Public Health Agency, National Tuberculosis Reference Laboratory, Ankara, Turkey, MTB H37Rv was used as the standard strain. The antimycobacterial activity results are summarized in Table 3.

2.3. *In silico* ADME/tox prediction

Discovery Studio Client 3.5 (Accelrys Software Inc, 2012) was used to examine the important ADME properties of benzimidazole derivatives. Lipinski's rule of five (Lipinski, 2004) was studied in the first step of understanding the compounds' druggability.

This software lightens the molecular properties and gives predictions on the compound's toxicity. Results on aqueous solubility, blood-brain barrier penetration, CYP2D6 binding, hepatotoxicity, intestinal absorption, and plasma protein binding were generated by the ADMET module of Discovery Studio Client 3.5 in the second step. Toxicity prediction was carried out with the explanation of some mutagenicity, carcinogenicity, tolerated dose, and biodegradability features of derivatives by the ADMET module.

2.4. Inverse virtual screening by molecular docking

Although it is known that benzimidazole derivatives interact with DprE1 (Verma et al., 2021), the interaction of molecules with 3 different target proteins (Arabinosyltransferase C (EmbC) (Nisha et al., 2020), (Filamentous Temperature Sensitive Mutant Z (FtsZ) (Akinpelu et al., 2020b), and Protein Tyrosine Phosphatase B (PtpB) (Thanh et al., 2019)) was investigated using the inverse docking approach (Sayed et al., 2020). FtsZ, EmbC, DprE1 are active enzymes in MTB cell wall synthesis. Cell wall synthesis is very important for the development of antibiotic resistance (Sarkar et al., 2017). For this reason, it is aimed to develop an inhibitor that will inhibit cell wall synthesis and these targets have been studied. In addition, studies show that FtsZ (Akinpelu et al., 2020a), DprE1 (Stanley et al., 2012), and PtpB (Sparks et al., 2007) interact with benzimidazole derivatives are available in the literature. In this way, it was aimed to determine the anti-tubercular activity of the compounds through the interaction with protein. The molecular docking process was carried out using AutoDock Vina, but firstly, ligand and receptor structures were prepared for this process.

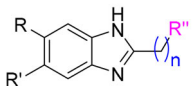
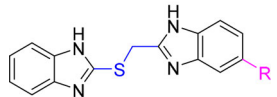
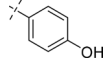
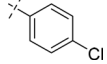
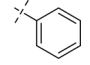
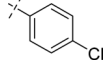
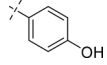
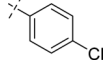
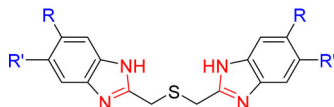
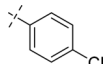
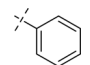
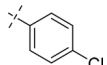
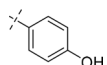
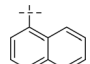
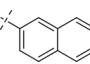
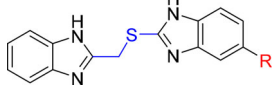
2.4.1. Ligand preparation

ChemSketch (Advanced Chemistry Development Inc, 2001) was used to draw 3D structures of ligands, which is given in Table 1, and ligands in crystal structures of the receptors (AFO, citrate, OMTS, O95). The conformations were fixed with the clean geometry option of this package. Then, one by one, the prepared ligand files were opened using the ligand module of the AutoDock tools package. Gasteiger charges and nonpolar hydrogen atoms were assigned automatically, and ligand input files were saved in PDBQT format for docking procedure by this module.

2.4.2. Receptor preparation

There are no mutations in the polymer sequences that are engineered from the reference sequence in proteins. Regions with missing and established cloning or expression tags are not located in active regions of proteins. Regions with missing and established cloning or expression tags were examined by Discovery Studio Client 3.5, no such missing residues were

TABLE 1. The structures of the final candidate compounds.

1 st , 2 nd , 3 rd group compounds					4 th group compounds	
						
Comp.	n	R	R'	R''	Comp.	R
12	1	H	H		30	H
13	1	H	H		31	Cl
14	1	Me	H		32	Br
15	1	Me	H		33	Me
16	1	Cl	Cl		34	F
17	1	Cl	Cl		5th group compounds	
						
18	2	H	H		Comp.	R
19	2	Me	H		38	H
20	2	Cl	Cl		39	Me
21	2	Cl	Cl		40	Cl
22	0	H	H		41	F
23	0	H	H		6th group compounds	
						
					Comp.	R
					45	Cl
					46	NO ₂

found in the active regions of the proteins. Afterwards, the prepared receptor file was opened with the Grid/Macromolecules module of the AutoDock tools package (Trott & Olson, 2010). Gasteiger charges and polar hydrogens were assigned automatically, and the receptor input file was saved in PDBQT format for docking procedure by this module.

2.4.3. Docking protocols for 4 protein targets

AFO, citrate, OMTS, O95 molecules were chosen as the center of the boxes. In Figure 1, the DprE1 enzyme, in which the grid box is formed by centering O95, is given. The docking area was defined using the grid/grid box module of the

AutoDock tools package. Docking Grid box properties determined for 4 protein targets are given in Table 2. Local Search Global Optimizer in AutoDock Vina was used to search docking conformations of ligands in the receptor's binding sites.

The docking output files were saved in log format for binding affinity (kcal/mol) calculations and PDBQT format for different conformations of ligands.

Docking, models the chemical properties that determine the binding conformation preference and binding free energy. It usually uses a scoring function for this purpose. This scoring function is a sum of intermolecular and intramolecular contributions in the AutoDock Vina algorithm (Trott & Olson, 2010). AutoDock Vina gives a binding affinity value

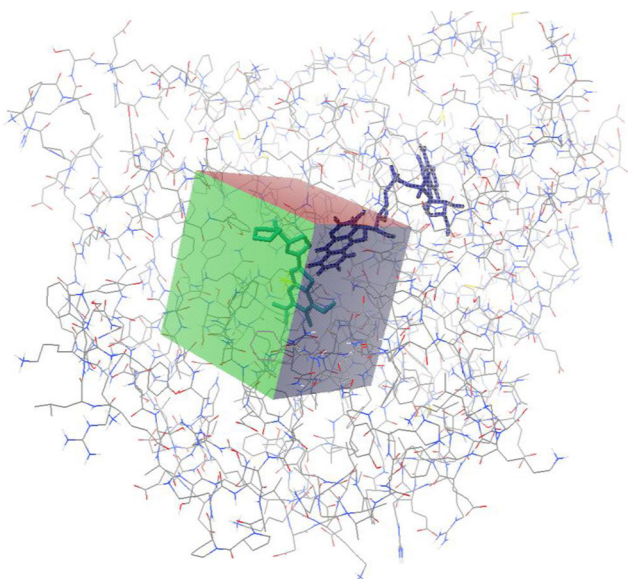


Figure 1. Atomic demonstration of decaprenylphosphoryl- β -D-ribose 2'-oxidase (DprE1). Grid box (cube) of docking protocol. x, y, z dimensions are given in blue, red, and green colors, respectively. O95, which is in the center of the box, is represented by light blue color. Flavin adenine dinucleotide (FAD) molecule is shown in dark blue.

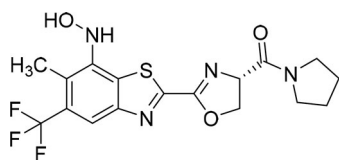
(kcal/mol). This value represents the binding energies of all conformations in the cluster (Nguyen et al., 2020). Negative Gibbs free energy (ΔG) scores (kcal/mol) calculated based on the AutoDock Vina scoring function are predicted as ligand binding affinities (Afriza et al., 2018; Sayed et al., 2020).

The analyze module of the AutoDock tools package was used for analyzing docking results by output files saved in PDBQT format. Moreover, Discovery Studio Client 3.5 and Chimera (Pettersen et al., 2004) were used for further analysis and detailed interactions.

2.5. Further in silico studies with DprE1

2.5.1. Docking with CDOCKER module of discovery studio client 3.5

Figure 2A–C shows the atomic coordinates of DprE1 from MTB, which was deposited in the Protein Data Bank (PDB; www.rcsb.org) accession no: 4P8H (Neres & Cole) for the structure at pH 7.2. DprE1 was co-crystallized with cofactor flavin adenine dinucleotide (FAD) and a receptor inhibitor, O95 ((4S)-2-[7-(hydroxyamino)-6-methyl-5-(trifluoromethyl)-1,3-benzothiazol-2-yl]-4,5-dihydro-1,3-oxazol-4-yl](pyrrolidin-1-yl)methanone) molecule.



O95 structure

The receptor was crystallized in dimer form and firstly Chain B was removed (Figure 2B). All other heteroatoms (i.e.

nonreceptor atoms such as water, ions, co-crystallized ligand) were also removed, except the FAD molecule because of its proximity to the active site (Maharaj et al., 2015). Hydrogens were added and their positions were fixed by Discovery Studio Client 3.5, with the use of CHARMM force field and the adopted basis set Newton–Raphson (ABNR) method.

Table 1 shows the ligands that were sketched by ChemSketch. Using the Discovery Studio Client 3.5, hydrogens were added. CHARMM force field parameterization was implemented to all atoms and then minimized using the ABNR method. With a temperature of 700K, ligands were heated and then annealed to 200K using a small simulated annealing molecular dynamics (MD) approach.

Discovery Studio Client was used to perform the CDOCKER protocol. Ligands were allowed to be flexible during refinement. First, O95 was docked, and root mean square deviation (RMSD) values were calculated to fix the binding sphere and docking protocol. RMSD enables the determination of ball poses with the highest energetic scores by comparing the different conformations of ligands at different dock poses with the initial conformation (biological configuration of the ligand). The RMSD value used when comparing the 3D structures of proteins was more clearly determined as 2 Å (Carugo & Pongor, 2001). In the comparison of the 3D structures of ligands, different values have been reached in the literature. However, the highest value was determined as 5 Å (Ravindranath et al., 2015; Singh et al., 2017).

CDOCKER method was implemented by default parameters. The 'exposure cluster radius' was defined to be 0.5 Å to increase the variety of fixed exposures. Top Hits was set to 20. 20 conformations were recorded for each ligand based on CDOCKER negative energy score and ranking. Binding energy was calculated with the 'Generalized Born with Molecular Volume' implicit solvent model following an ABNR in situ ligand minimization process with 1000 steps, 0.001 RMS gradient. As shown in Figure S1, the docking sphere for x, y, and z coordinates was chosen as -17.09 , -19.84 , 1.08 , respectively, with 9.74829 Å radius value.

2.5.2. MD Simulations

MD simulations were implemented to five benzimidazole derivatives (16, 19, 20, 21, and 30) that gave the best docking scores. AMBER 14SB (Maier et al., 2015) and AMBER Gaff forcefields (Case et al., 2014) were used to parameterize the final coordinates of the protein-ligand systems. Furthermore, protonation, ion addition, and solvation of the initial structures were implemented by the leap module of AMBER v14 (Case et al., 2014). To constitute an octahedral water box, the protein-ligand complex was solvated in LEAP by putting together small units of TIP3 water boxes in dimensions of $95.098 \text{ \AA} \times 95.098 \text{ \AA} \times 95.098 \text{ \AA}$ (Figure S2). Solvent unit box means the box size of 216 water molecules (WATBOX216) that will be used to overlay the solute, remove water molecules that are too close to or inside the solute, and be trimmed to the desired size. The distance between the outer boundary of the octahedral solvent box and the solute surface was set to 8 Å. To set water molecules at the solute-solvent boundary, a space of 0.4 Å was used. PMEMD module

TABLE 2. Grid Box properties of target proteins.

Receptor	PDB ID	X center	Y center	Z center	Grid Point	Dimensions
Arabinosyltransferase C	3PTY (Trott & Olson, 2010)	3.519	10.687	93.867	0.375 Å	40 Å × 40 Å × 40 Å
FtsZ	1RQ2 (Alderwick et al., 2011)	-8.621	41.263	3.538	0.375 Å	30 Å × 30 Å × 30 Å
PtpB	2OZ5 (Leung et al., 2004)	5.361	60.884	6.14	0.375 Å	40 Å × 40 Å × 40 Å
DprE1	4P8H (Grundner et al., 2007)	-19.957	-21.982	0.829	0.375 Å	30 Å × 30 Å × 30 Å

TABLE 3. The minimum inhibitory concentration (MIC) values ($\mu\text{g/mL}$) of compounds against the *Mycobacterium tuberculosis*.

Compounds	<i>M. tuberculosis</i> H37Rv	Compounds	<i>M. tuberculosis</i> H37Rv	Compounds	<i>M. tuberculosis</i> H37Rv
12	62,50	20	3,90	34	31,25
13	31,25	21	7,81	38	31,25
14	31,25	22	62,50	39	31,25
15	15,625	23	31,25	40	31,25
16	31,25	30	3,90	41	31,25
17	15,625	31	31,25	45	31,25
19	15,625	32	31,25	46	31,25
18	31,25	33	31,25	Isoniazid	0,97
				Ethambutol	1,95

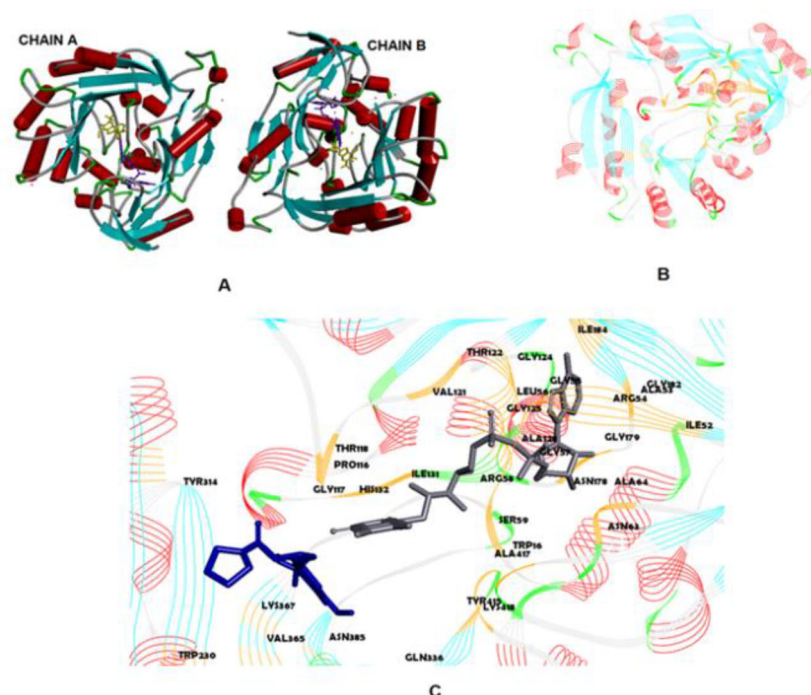


Figure 2. Crystal structure of DprE1; (PDB ID: 4P8H). (A) Schematic demonstration of receptor in dimer form (Chain A and Chain B) with ligands [flavin adenine dinucleotide (FAD), O95] and water molecules (red dots). (B) Line ribbon demonstration of Chain A; orange parts show the receptor's active site. (C) Demonstrations of FAD (gray) and O95 (blue) in the active site. Residues in the active site were shown in orange and labeled with residue names. Residues of the active site were analyzed for hydrogen bonds, π - π interactions, and close relationships to the visualization of potential binding conformations of ligands. FAD residue was also examined because of its proximity to the binding site as shown in Figure 2.

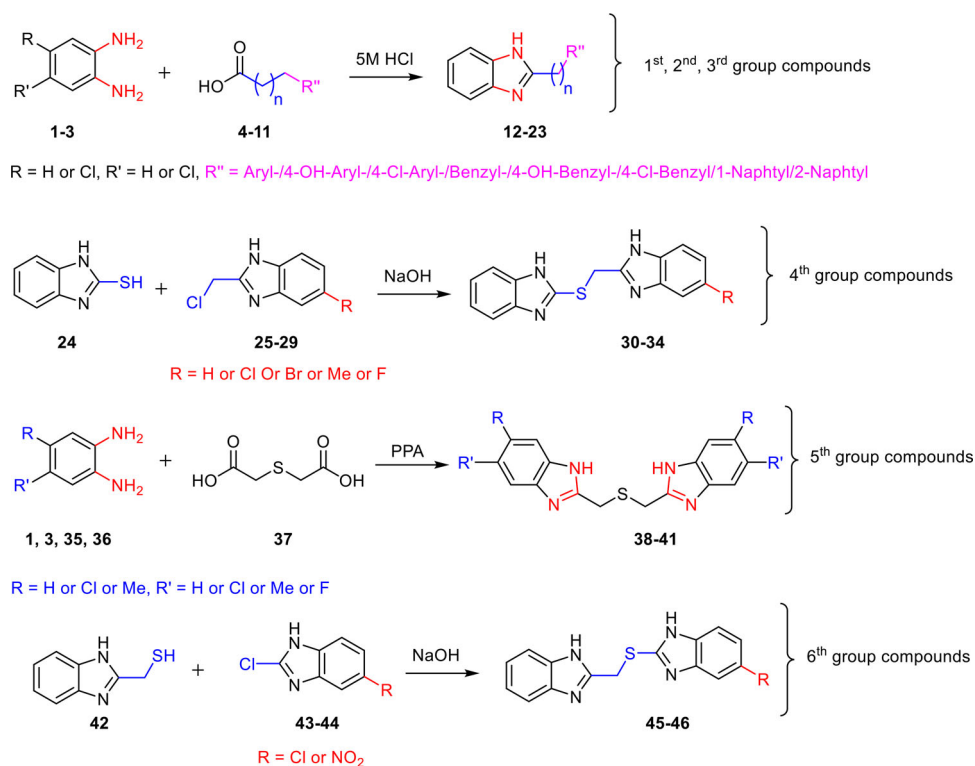
of AMBER v14 was used to implement relaxation and temperature equilibration of the solvated complex structure, and the pmemd.cuda module was used for parallel implementation of explicit solvent MD computations (Götz et al., 2012; Salomon-Ferrer et al., 2013). Calculations were conducted at the TR-Grid e-Infrastructure of Turkey.

The protein-FAD-ligand systems were preheated up to 298.15 K over 100 ps (50,000 iterations and 2 fs for each of them) during which the protein and the ligand were strongly restrained. Finally, with no restrains, at least 100 nsec of production MD runs were implemented for the complex systems at 1 bar and 298.15 K, which utilized the Langevin dynamics algorithm (with a collision frequency of 1 ps^{-1} and a velocity limit of 10 Kelvin) in keeping the temperature constant and SHAKE algorithm.

3. Results

3.1. Synthesis of the final candidate compounds 12–23, 30–34, 38–41, 45 and 46

Methods in the literature reported that five groups of compounds were successfully synthesized (Akpa et al., 2016; Ayaz et al., 2020; Boggu et al., 2016; Duran et al., 2020; Ersan et al., 2020; 2021; Gozelle et al., 2019; Gümüs et al., 1989; Niknam & Fatehi-Raviz, 2007; Oren et al., 1997; Phillips, 1928; Wang et al., 2006). Scheme 1 illustrates the general synthetic pathways for the preparation of final candidate compounds. Compound 21 is the only newly synthesized among the selected compounds. With this, a mixture of 4,5-dichloro-1,2-phenylenediamine derivative (1 eq) and 4-hydroxyphenylpropionic acid (1.1 eq)



Scheme 1. General synthetic pathways for preparation of candidate final compounds

was refluxed for a period of 15 h in 5 M hydrochloric acid. To get the precipitate, the reaction mixture was poured onto ice water and neutralized by mixing with NaHCO₃ until slightly basic pH = 8. The resulting precipitate was filtered off and washed with cold water, and then recrystallized with a suitable solvent system (ethanol-water). The resulting crystalline compounds were filtered, and the vacuumed product was dried. Compound **21** was obtained as a brown solid. Yield 71% (0.65 g); m.p. 249–251 °C; IR (KBr, cm⁻¹) ν_{max} 3366, 3142, 1449, 1243, 821; ¹H NMR (400 MHz, DMSO- d₆) δ 7.98 (s, 2H), 7.04 (d, J = 8.50 Hz, 2H), 6.69 (d, J = 8.50 Hz, 2H), 3.26 (t, J = 7.75 Hz, 2H), 3.07 (t, J = 7.75 Hz, 2H); ¹³C NMR (100 MHz, DMSO- d₆) δ 156.8, 155.9, 133.8, 129.8, 129.0, 126.3, 115.6, 115.3, 31.74, 29.5; LC-MS/MS (ESI+): m/z = 307.1 ([M + 1]⁺).

IR, MS, ¹H NMR, and ¹³C NMR spectroscopy were used to confirm the structures of all compounds. The structures of the final candidate compounds are shown in Table 1.

3.2. Antitubercular studies

The agar proportion method was used to screen all target compounds against MTB H37Rv (Burmaoglu et al., 2017; Maia et al., 2020). INH and EMB were used as the positive drug standards for the assay. Table 3 shows the *in vitro* antimycobacterial activity in terms of the MIC values of the target compounds and standard drugs. The three benzimidazole and bisbenzimidazole derivatives, **20**, **21**, and **30**, show significant activities and other compounds exhibit moderate activities.

3.3. Computational studies

The drug development process involves long, comprehensive, and complex strategies. Among the accepted techniques in

accelerating drug development processes, are computational modeling techniques, molecular docking, pharmacokinetic profile (ADME), and recent advances in the analysis of toxicity and bioavailability of molecules (Genheden et al., 2010). Besides, the integration of MD simulation provides accuracy on the spatial fitting, interaction stability, and binding affinity of ligands at the protein's active site (Batt et al., 2012; Kumari et al., 2014; Wang & Hou, 2012).

Here, a new strategy based on molecular docking is applied by using both the AutoDock Vina and CDOCKER method and MD simulations and ADME properties of compounds for DprE1.

The active molecules which were against the oxidoreductase enzyme involved in cell wall synthesis of MTB in literature led to the selection of benzimidazole compounds (Manjunatha et al., 2019; Stanley et al., 2012). For DprE1 inhibitors, ADME, toxicity, and pharmacokinetic profile analyses were performed on potential lead molecules. For DprE1 inhibitors, ADME, toxicity, and pharmacokinetic profile analyses were performed on potential lead molecules. Multiple MD simulations were carried out on DprE1, DprE1-**095**, and DprE1-benzimidazole compound complexes to improvise molecular docking results. The structural stability of protein-ligand interaction, conformational orientation, stability, and molecular interactions of ligands at the active site are typically deciphered by MD simulations (Panda et al., 2014; Prakash & Luthra, 2012; Sastry et al., 2013). For this purpose, the focus of this study was on RMSD, RMS fluctuations (RMSF) calculations, and hydrogen bond analysis of MD simulations with post trajectory processes.

3.3.1. *In silico* ADME/tox prediction

Molecular properties of benzimidazole derivatives such as AlogP, molecular weight, number of aromatic rings, number

TABLE 4. ADME properties of benzimidazole derivatives.

	AlogP ^[a]	Solubility-level ^[b]	CYP2D6 Prediction	Absorption-level ^[c]	PPB Prediction	PSA_2D
12	3,063	3	False	0	False	47,131
13	3,969	2	True	0	True	26,316
14	3,549	2	False	0	True	47,131
15	4,455	2	True	0	True	26,316
16	4,392	2	False	0	True	47,131
17	5,298	1	True	0	True	26,316
18	4,426	2	True	0	True	26,316
19	4,912	2	False	0	True	26,316
20	5,754	1	True	0	True	26,316
21	4,848	2	False	0	True	47,131
22	4,213	2	True	0	True	26,316
23	4,213	2	True	0	True	26,316
30	3,721	2	False	0	True	52,632
31	4,385	1	False	0	True	52,632
32	4,469	1	False	0	True	52,632
33	4,207	2	False	0	True	52,632
34	3,926	2	False	0	True	52,632
38	4,128	2	False	0	True	52,632
39	3,866	2	False	0	True	52,632
40	3,79	2	False	0	True	52,632
41	3,585	2	False	0	True	52,632
45	4,044	2	False	0	True	52,632
46	3,379	2	False	0	True	52,632
095	3,204	2	False	0	True	85,793

[a] AlogP, the logarithm of the partition coefficient between n-octanol and water; [b] Aqueous solubility level: 0 (extremely low); 1 (very low, but possible); 2 (low); 3 (good); [c] Human intestinal absorption level: 0 (good); 1 (moderate); 2 (poor); 3 (very poor).

of H-acceptors, number of H-donors, number of rings, number of aromatic rings, number of rotatable bonds, and molecular fraction polar surface area are calculated using the 'calculate molecular properties module' of the Discovery Studio v3.5. Results are given in Table S1. It is shown that whole ligands are found to pass the Lipinski rule of five (Table S1).

The ADMET descriptors module of the Discovery Studio Client 3.5 was used to determine ADME prediction. Key values such as 'AlogP value, human intestinal absorption, solubility, CYP2D6 binding, plasma protein binding' are given in Table 4. The solubility of each compound in the water at 25 °C is provided by aqueous solubility. Compound **12** (level 3) was determined to be the most solvable compound, however, most of the compounds show low solvability with level 2. Compound **20** showed the highest lipophilicity because of its highest log P value. Especially expressed in the liver, CYP2D6 is a key enzyme for drug metabolism and elimination. CYP2D6 binding predicts cytochrome P450 2D6 enzyme inhibition for 24 compounds. Most of the compounds, especially group 5, were found no inhibitors for CYP2D6. Absorption levels of whole ligands were found good for human intestinal system absorption. Plasma protein binding is an important parameter in predicting the drug distribution via the compounds' binding profile to carrier proteins in the blood. All ligands except **12** were found to be highly bound with plasma proteins. Compounds **16**, **19**, **21**, and most of group 5 were found within the acceptable range for human beings (Table 4, Figure S3). Figure S3 shows the different features of compounds because of their difference in lipophilicity rather than their 2D polar surface area. Compound **20** is much lipophilic (logP > 5), which is not propitious for a good oral bioavailability, as opposed to compound **12**. Compounds having lower lipophilicity (logP < 3.4) are predicted to be very well-absorbed.

3.3.2. Inverse virtual screening by molecular docking

Docking was performed with all the ligands given in Table 1 and the best docking results were obtained at compounds **13**, **30**, and **39** for EmbC, compounds **16**, **33**, **39** for FtsZ, compounds **13**, **16**, **33** for PtpB, and compounds **20**, **21**, **30** for DprE1 (Table 5). Although it was determined that the compounds **20**, **21**, and **30** showed a significant interaction with DprE1 compared to the docking results obtained with the X-ray ligand (**095**), the same results could not be obtained with the other 3 protein targets.

The binding profiles of the proteins as a result of docking with X-ray ligands are given in Figure 3. Interactions between PtpB and OMTS were given in Figure 3a. Five hydrogen bonds (4 conventional bonds, 1 carbon-hydrogen bond) were generated with ALA162, LYS164, ASP165 residues of PtpB. Interactions between FtsZ and citrate were given in Figure 3b. Two conventional hydrogen bonds were generated with ASN740 residue of FtsZ. Interactions between EmbC and AFO were given in Figure 3c. Seven conventional hydrogen bonds were generated with GLY105, THR106, GLY19, GLY107, GLY18 and ASN41 residues. The binding profiles given in Figure 3 show that the ligands are tightly packed within the binding site.

The binding profile of the receptors with the ligands with the highest dock score is given in Figure 4. There are two π interactions between LYS164, ASP165 residues of PtpB and compound **16**. Two π interactions were generated between ASP1051 residue of FtsZ and compound **39**. Three conventional hydrogen bonds were generated with GLY105, THR106, GLY19, residues of EmbC and compound **13**.

3.3.3. Comparative molecular docking analysis for the DprE1 enzyme

In this study, in the examination of the interaction of the DprE1 enzyme, a single molecular docking algorithm was not

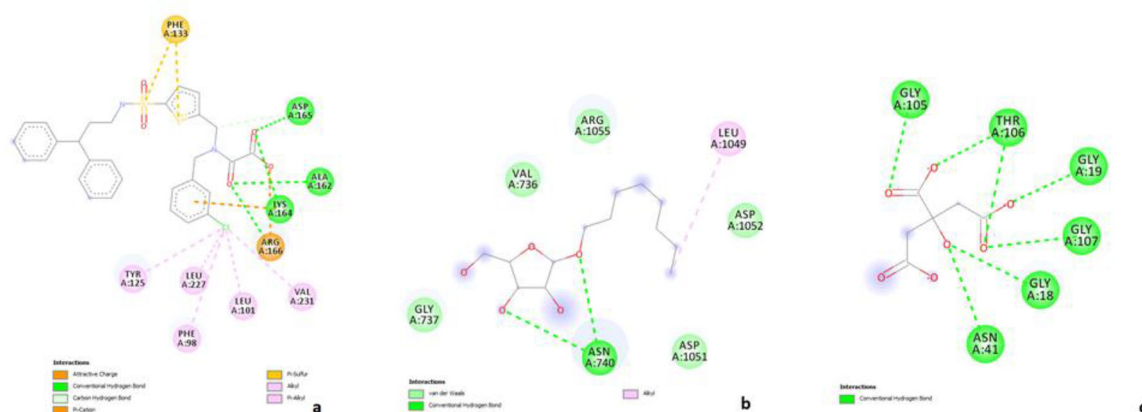


Figure 3. The binding profile between proteins (EmbC, FtsZ, PtpB) and X-ray inhibitors. A) Interactions between PtpB and OMTS. B) Interactions between FtsZ and citrate. C) Interactions between EmbC and AFO.

TABLE 5. Best docking results for 7 ligands with the highest binding affinity for all target proteins.

Compounds	Binding Affinity (kcal/mol)			
	EmbC	FtsZ	PtpB	DprE1
13	-5.9	-5.1	-7.4	-7.7
16	-4.9	-5.4	-7.8	-8.0
20	-5.0	-4.6	-7.0	-8.6
21	-4.7	-4.6	-6.9	-8.5
30	-5.7	-4.4	-6.4	-8.2
33	-4.5	-5.7	-7.1	-6.7
39	-5.4	-6.0	-7.0	-7.4
AFO	-9.7	-	-	-
citrate	-	-9.4	-	-
OMTS	-	-	-10.9	-
O95	-	-	-	-9.4

adhered to, and separate molecular docking was performed with AutoDock Vina and CDOCKER. In this section, the results are given for all molecules comparatively.

In this study, 23 new benzimidazole derivatives were docked into DprE1 (PDB ID: 4P8H (Neres & Cole)). As seen in Figure 2C, DprE1's binding pocket includes ARG 413, SER 228, GLN 336, GLN 334, ASN 385, TYR 314, TRP 230, LYS 134, HIS 132, LYS 418, TYR 60 residues (Panda et al., 2014).

Figure 5 and Table 6 illustrates the binding features between **O95** and DprE1. RMSD (~ 2 Å) values of the inhibitor compound (**O95**) were found reliable for both docking methods (Table 6). Hydrophobic residues of the active site (HIS 132, SER 228, TRP 230, CYS 387, ARG 413, AND LYS 418) cover the whole around of the benzothiazole ring of **O95** (Figure 5). Possible H bonds are formed between the hydroxy amino group of the benzothiazole ring of LYS 418 (distance = 2.58 Å) and ASN 385 residues. The sulfur of the benzothiazole ring generates an H bond with the amino group of LYS 418 (distance = 3.14 Å). The oxygen of the oxazoline ring generates an H bond with LYS 418 and TYR 60 (Figure 5).

The superposition of X-ray coordinates and best docking results (2.0601 Å) are given in Figure 6. Overlapping of two modes **O95** gives a reason for understanding the docking protocol's stability.

The ligands shown in Table 1 were also docked into the binding pocket with AutoDock Vina and CDOCKER. Figure 7 shows a correlation between residues of interest and molecules generating H bonds in the enzyme's active site by molecular

docking with AutoDock Vina. Although SER 228, TYR 314, and ASN 385 residues were found important for H bonds and TRP 230 residue was found essential for π - π interaction, LYS 418 residue was found crucial for both binding profiles. Thirteen molecules (**12**, **13**, **15**, **16**, **17**, **23**, **31**, **34**, **38**, **39**, **40**, **45**, and **46**) of the 23 new inhibitor benzothiazole derivatives create π - π interaction with LYS 418 residue. The other π - π interaction center was found as an indole ring of TRP 230 residue which generates two π - π interactions in every two rings of this group.

Surprisingly, the FAD molecule was found effective on the ligands' binding profile. Three of the inhibitor molecules generate an H bond with the isoalloxazine ring of FAD.

Table 7 shows the binding properties of interested molecules on AutoDock Vina results. Conformational changes on receptor protein are generated by the binding of drug molecules and because of this, special energy comes out. This energy change gives binding affinity for drug molecules. Table S2 shows the 20 different binding modes predicted for every 23 molecules, and the best docking conformations having the smallest binding affinity scores are given in Table 4. RMSD (~ 3 Å) values of the whole benzimidazole derivatives were found reliable. As indicated in Table 7, compound **20** has the best binding affinity (-8.6 kcal/mol) and inhibitory constant (0.497 μ M).

Figures 8–10, S4 and S5 shows the AutoDock Vina docking results and indicates that compounds **20**, **21**, and **30** provide the best binding properties as binding affinity value and bonding features. As observed in Figures 8, 9, and S4, NH of benzimidazole ring of **20** and **21** is found to be H bond donors, which generate H bond with the oxygen of carbonyl of TYR 314 residue. On the other hand, pyridine N atoms of **20** and **21** participated in the H bond as an acceptor for interacting with SER 228 and benzimidazole showed π - π interactions with TRP 230 residue.

Compound **21** showed a binding affinity score of -8.5 kcal/mol (Table 7), and the same binding profile as compound **20** was seen for this ligand as well (Figure 10). Compound **30**, with -8.2 kcal/mol, has the third-best binding affinity score (Table 7). As seen in Figures 10 and S4, compound **30** showed the same binding profile. According to this result, it can be concluded that it is not important to have two benzimidazole rings in the same molecule in binding active residue.

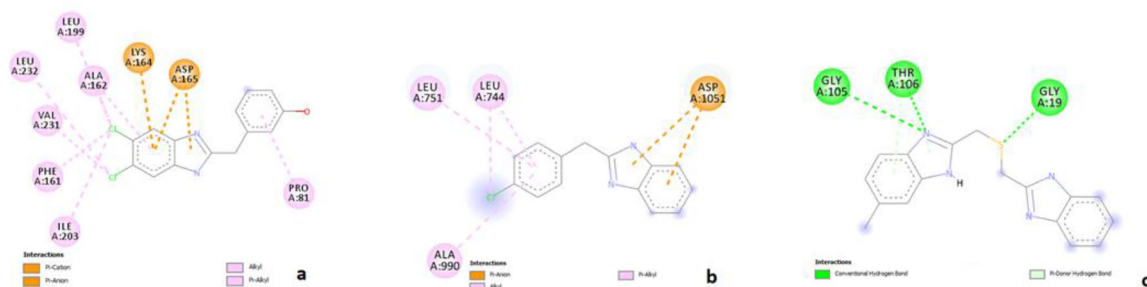


Figure 4. The binding profile between proteins (EmbC, FtsZ, PtpB) and the inhibitors with top binding affinities. A) Interactions between PtpB and compound 16. B) Interactions between FtsZ and compound 39. C) Interactions between EmbC and compound 13.

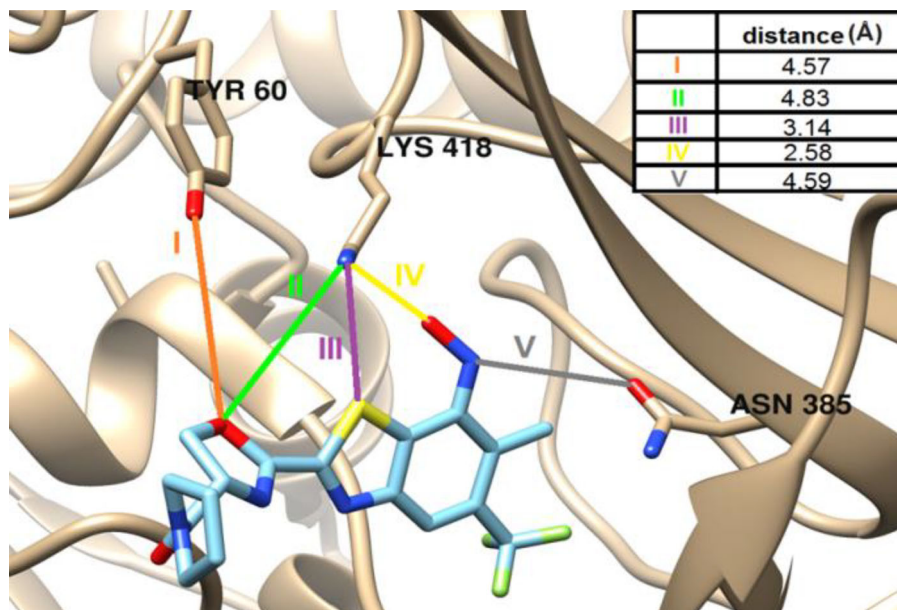


Figure 5. Interaction of **O95** (blue molecule) with DprE1. This H bond analysis was generated with Chimera. (Relax H bond constraints: 2.5 Å, 20°) Bond distances were given in a small table.

TABLE 6. The binding affinity values of different poses of predicted **O95** by AutoDock Vina and CDOCKER.

AutoDock Vina		Distance from best mode (Å)		CDOCKER
Mode	Affinity (kcal/mol)	RMSD l.b.	RMSD u.b.	
1	-9.4	0.000	0.000	2.0601
2	-9.1	2.132	2.765	2.0608
3	-8.8	2.047	3.370	2.0589
4	-8.6	2.232	3.757	2.1031
5	-8.2	4.307	6.226	2.1031
6	-8.1	3.063	4.716	2.1031
7	-7.9	2.999	3.619	2.1031
8	-7.6	2.998	3.748	2.1031
9	-7.4	3.075	4.525	2.1031
10	-7.2	2.729	3.602	2.1031

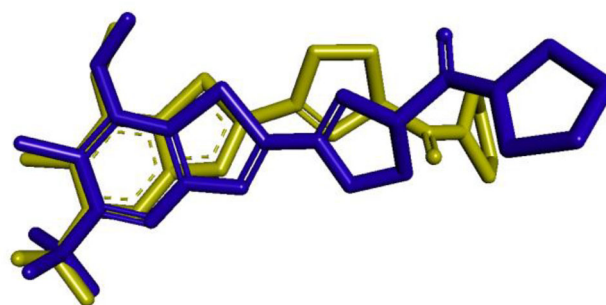


Figure 6. Superposition of X-ray coordinates and best docking result of **O95**. Yellow demonstrates the X-ray version of **O95**, whereas blue demonstrates the docking result.

Table 7 shows that the third-best binding affinity score is from compounds **16** and **19**, with -8.0 kcal/mol. π - π interaction was shown between the benzimidazole rings of compound **19** and TRP 230 residue as seen in Figure S6. Moreover, nitrogen atoms of the benzimidazole ring generate an H bond with SER 228 and TYR 314 residues. H bonds are formed between $-OH$ group of compound **16** and TYR 60, LYS 418 residues as seen in Figure S7. Moreover, one of

the chlorine atoms of the benzimidazole ring generates an H bond with ASN 385 residue.

Because of its multichannel structure, the receptor's binding pocket is found to be considerably large. Compared with **O95**, Figure 11 illustrates that the newly screened benzimidazole derivatives (**20** and **16**) are ensconced to different channels of the binding pocket. Different effects of functional groups in derivatives are shown in these results.

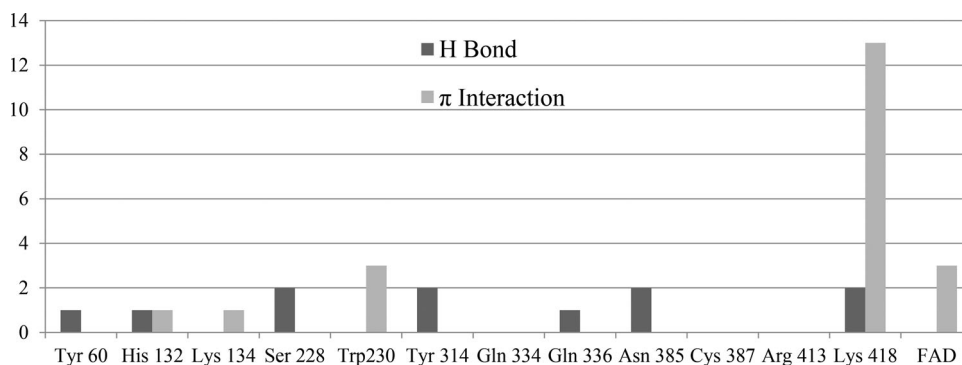


Figure 7. Binding profile of the residues of interest with inhibitor molecules of this work. Dark gray bars give H bond properties, while light gray bars give π interactions (π - π interactions, π -cation interactions).

TABLE 7. Binding affinities and inhibitory constants of the other molecules.

Comp. Code	Binding Affinity ΔG (kcal/mol)	Inhibitory constant K_i (μM)	Comp. Code	Binding Affinity ΔG (kcal/mol)	Inhibitory constant K_i (μM)
12	-7.8	1.917	30	-8.2	0.976
13	-7.7	2.269	31	-7.6	2.686
14	-7.3	4.457	32	-7.9	1.619
15	-7.3	4.457	33	-6.7	12.270
16	-8.0	1.367	34	-7.6	2.686
17	-7.5	3.180	38	-7.5	3.180
18	-7.4	3.765	39	-7.4	3.765
19	-8.0	1.367	40	-7.2	5.277
20	-8.6	0.497	41	-7.1	6.247
21	-8.5	0.588	45	-7.5	3.180
22	-7.1	6.247	46	-7.8	1.917
23	-7.9	1.619			

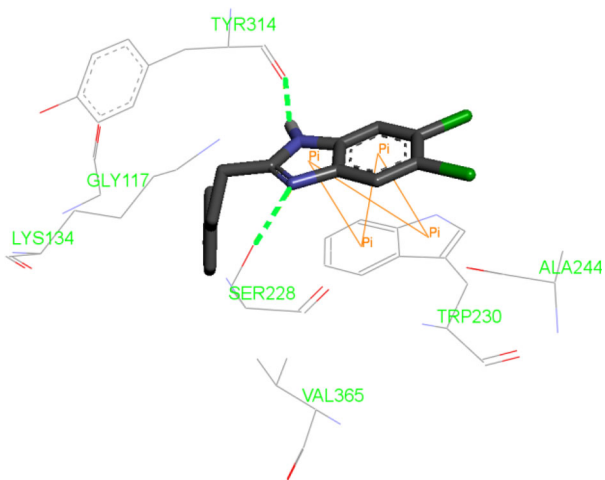


Figure 8. Binding features of compound 20. Green lines show H bonds. Orange lines show π - π interactions.

CDOCKER docking results for each ligand are given in Table 8. Best binding affinity values were taken by **21** (-31.9192 kcal/mol) and **30** (-33.2284 kcal/mol).

Figure 12 shows the binding profile of **30**. Because of the π -cation interactions between LYS134 and the benzimidazole ring, LYS134 is found as a key amino acid. The importance of LYS134 was determined by both AutoDock Vina and CDOCKER docking methods. HIS132 shows an H bond with the other benzimidazole ring just in CDOCKER docking results.

In the AutoDock Vina results, **21** showed the second-best binding affinity value. But **21** generated just an H bond with LYS 418 residue (Figure 13) with the difference of AutoDock

Vina docking profile (key residues were: TYR 314, TRP 230, SER 228).

Besides the comparison of calculated values, the superposition of docking results for CDOCKER and AutoDock Vina shows more same binding coordinates (Figure 14 and Table 9).

3.3.4. MD Simulations

Based on AutoDock Vina results (Table S2), the best-docked poses of **21**, **20**, **16**, **19**, and **30** were evaluated. Figure 15 is a plot of RMSD curves for ligand-FAD-protein complex for the five ligands. Taken as a reference in RMSD computations were the systems' initial coordinates. As seen in the figure, protein structure, as well as FAD and ligands, conformationally stabilize after 80 ns of MD. This means that the first 80 ns of MD is adequate to provide all the necessary information about the systems.

For the DprE1 protein structures, the RMSF of $C\alpha$ atoms from their time-averaged positions were analyzed, as shown in Figure 16. It is important to show the RMSF calculations because of the interacted residues. Fluctuated residues could demonstrate the ligand interacted residues. The protein was found to be stable and showed similar patterns during all five simulations of the DprE1-ligand-FAD complex. The highest atomic fluctuations in region 269-286 for DprE1 were observed to be correlated with its disorderness. This means all ligands affect the binding pocket of protein structure.

MD trajectory analysis was used to study the ligands' binding feature in complex with DprE1 and FAD. Results were examined for the whole 100 ns of simulation but

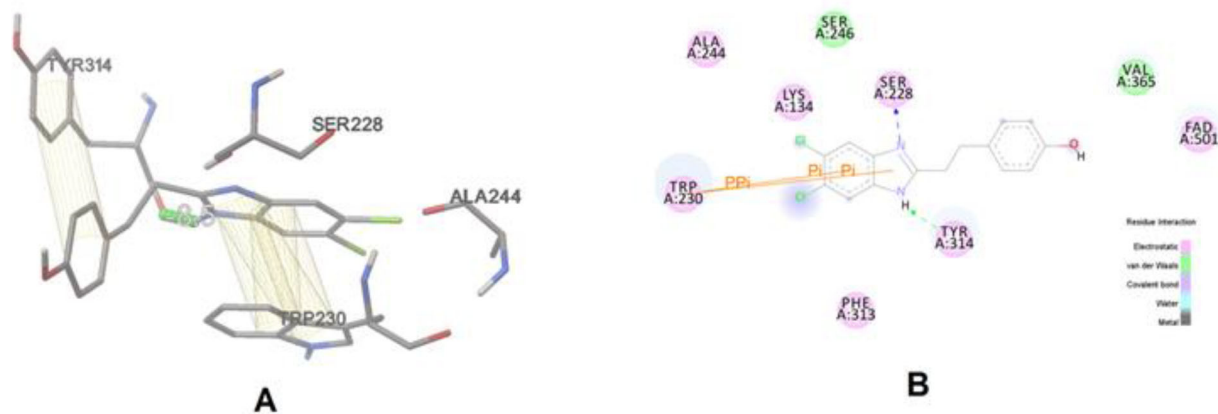


Figure 9. Dock result analysis of compound **21**. (A) Analysis with AutoDock tools. Green dots show H bond with TYR 314 residue; yellow parallels show π - π interaction with TRP 230 residue and TYR 314. (B) Analysis with AutoDock output file by Discovery Studio Client. Blue dots show H bond with SER 228, green dots represent another H bond with TYR 314, and orange lines show two π - π interactions between TRP 230 and two rings of the benzimidazole molecule.

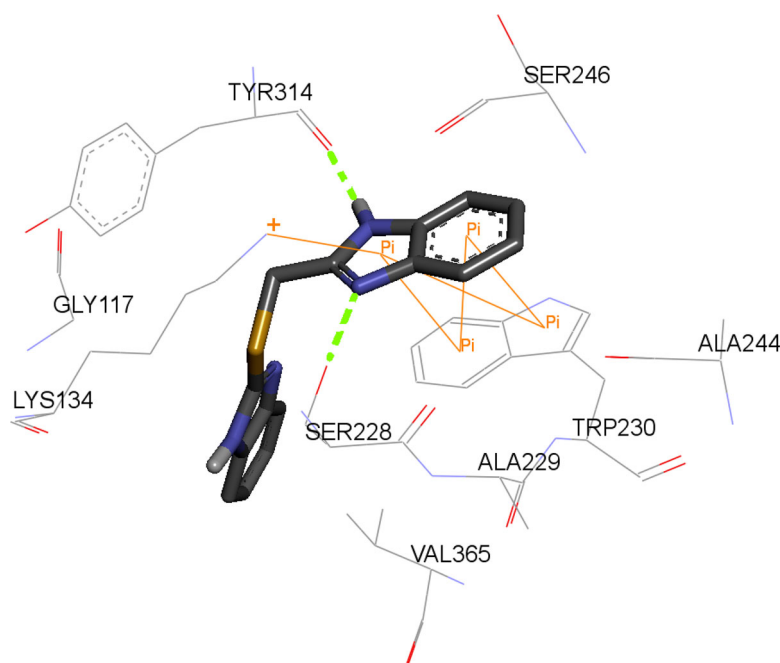


Figure 10. Binding features of compound **30**. Green lines show H bonds with TYR 314 and SER 228. The orange line shows π - π interactions between the benzimidazole ring of compound **30** and TRP 230.

exactly after 80 ns of simulation. Compounds **21** and **30** were found locked to DprE1's binding pocket throughout the whole simulation (Figures 17, 18, Figure S8, Video S1, Figure S9, Video S2), whereas the other ligand was moved away from receptor structure after 70 ns of simulation (Figures 19–21, Figure S10, Video S3, Figure S11, Video S4, Figure S12, Video S5). The hydroxyl group, which is connected to the benzene ring and NH of the benzimidazole ring was found to be the key group of **21** as in dock results. H bonds were generated between the hydroxyl group of the benzene ring, TYR 60 (2.08 Å), and LYS 418 (1.85 Å). As shown in Figure 17, NH of the benzimidazole ring also generates two bonds with GLN 336 (2.19 Å) and HIS 132 (1.98 Å).

Compound **30** has two benzimidazole rings. These two rings generate H bonds with their NH groups. In Figure 18, CYS387 (2.34 Å), LYS134 (2.34 Å), and ASP389 (2.39 Å) residues are observed to generate bonds in accordance with the literature and our docking results.

Compound **20** generates H bonds with GLY331, SER228, and LYS134; however, it moves away from the receptor after 70 ns of simulation (Figures 19, S10, and Video S3).

Compound **16** generates H bonds with HIS132, SER228, and PHE328; however, it moves away from the receptor after 80 ns of simulation (Figures 20, S11, and Video S4).

Compound **19** generates H bonds with GLN336 and PHE328; however, it moves away from the receptor after 83 ns of simulation (Figures 21, S12, and Video S5).

4. Discussion

MTB antimicrobial susceptibility testing (AST) can be conducted in two ways: 1) Macrobroth method with instruments such as BACTEC, VersaTREK or BacT/WARNING. 2) The agar proportion method was used in this study (Hall et al., 2011). Although isoniazid (INH) and ethambutol (EMB) are drug

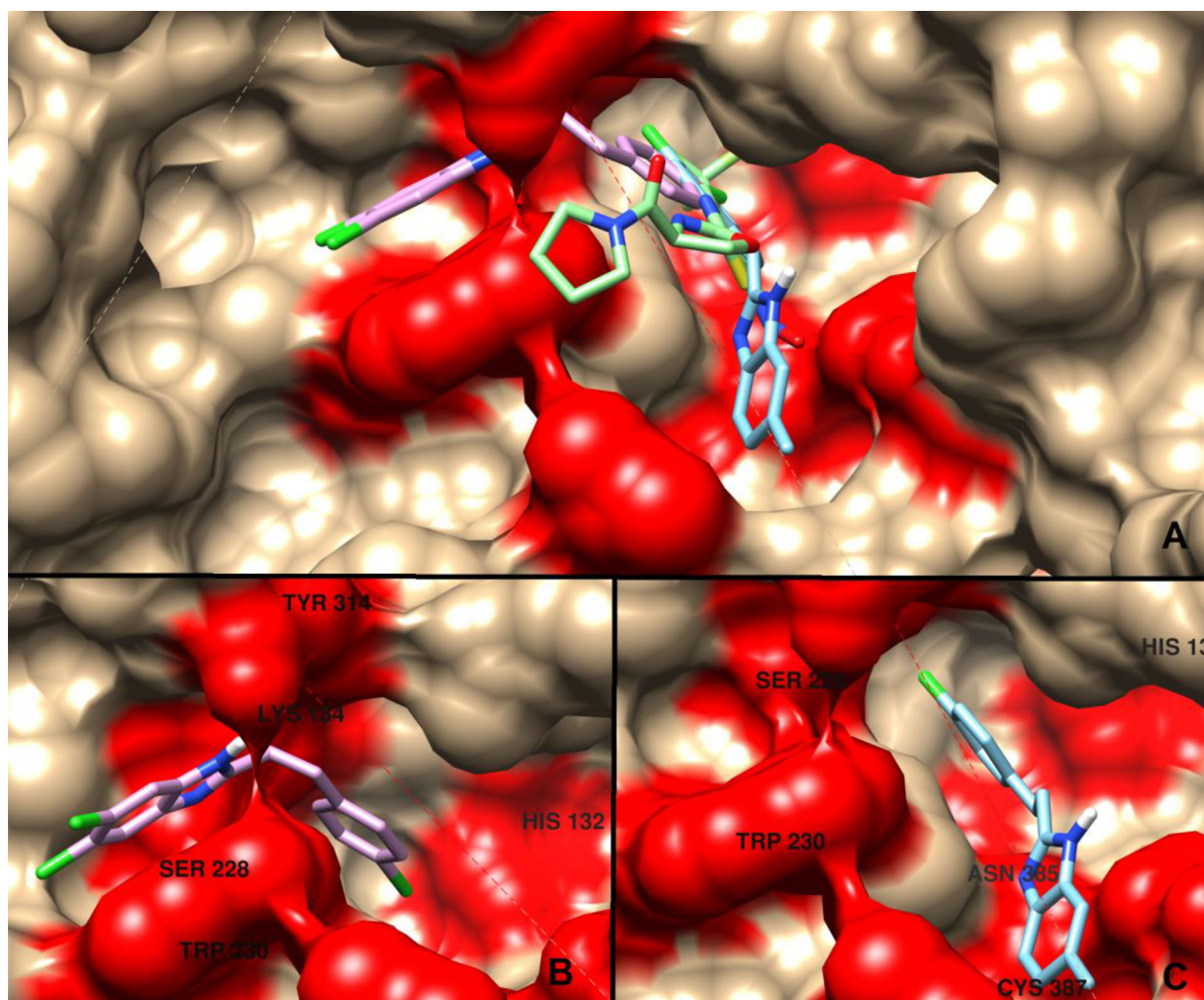


Figure 11. (A) Multi channelled binding pocket with 16 (blue), 20 (pink), O95 (green). (B) Interaction area of 20. (C) Interaction area of 16.

TABLE 8. CDOCKER results of 23 benzimidazole derivatives, and compound O95.

	Compound	Binding mode	Binding Energy (kcal/mol)	-CDOCKER ENERGY (kcal/mol)	-CDOCKER Interaction Energy kcal/mol)
1	12	5	-19,7857	27,0499	32,0108
2	13	5	-3,4579	19,9049	28,1146
3	14	8	-24,3578	25,7179	35,4238
4	15	2	-11,6159	22,9204	29,2364
5	16	1	-17,6604	22,6125	32,44
6	17	1	-18,2066	22,1864	33,009
7	18	6	-32,2089	20,5771	30,8386
8	19	6	-4,54733	29,5246	34,5097
9	20	1	-14,1752	27,0984	37,0133
10	21	5	-31,9192	28,4478	38,0772
11	22	1	12,3764	9,75838	28,466
12	23	1	-13,7465	17,2281	33,6365
13	30	1	-33,2284	18,5425	33,8963
14	31	1	-28,7754	21,3348	37,0083
15	32	5	-10,8705	20,0795	35,069
16	33	2	-28,3619	20,3747	34,922
17	34	1	-28,6226	19,9425	34,7813
18	38	5	-19,6393	26,063	36,3171
19	39	2	-16,9093	27,9117	37,0418
20	40	2	-19,4913	27,1554	37,5015
21	41	7	-11,5088	27,5044	37,699
22	45	1	-17,6049	38,8295	28,4915
23	46	3	-22,4002	26,8938	36,78
Reference	O95	1	-23,9306	-4,12728	45,849

Binding modes are also determined by CDOCKER.

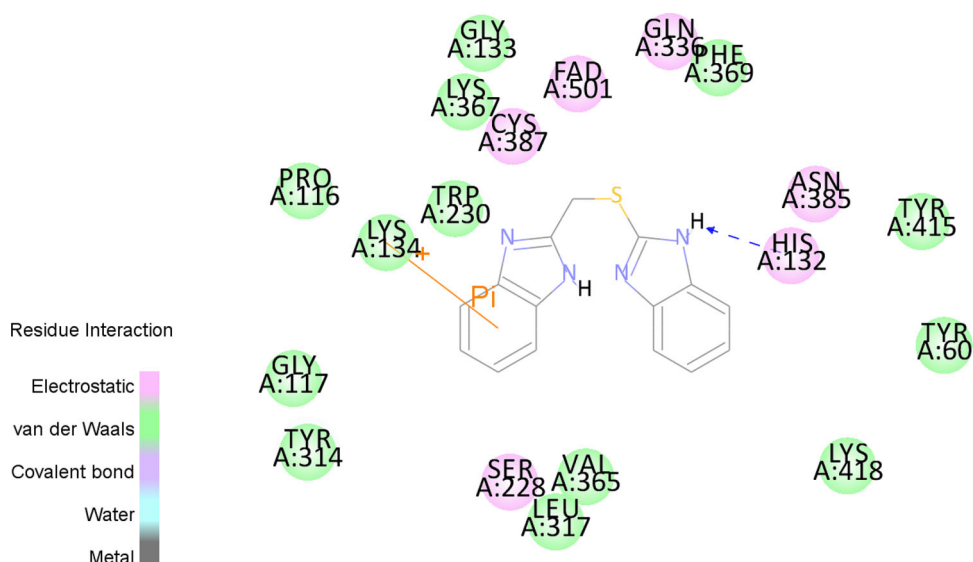


Figure 12. Binding analysis of 30 CDOCKER docking results. Blue dots show the H bond between HIS132 and the benzimidazole ring. The orange line shows π -cation interactions between LYS134 and the other benzimidazole ring.

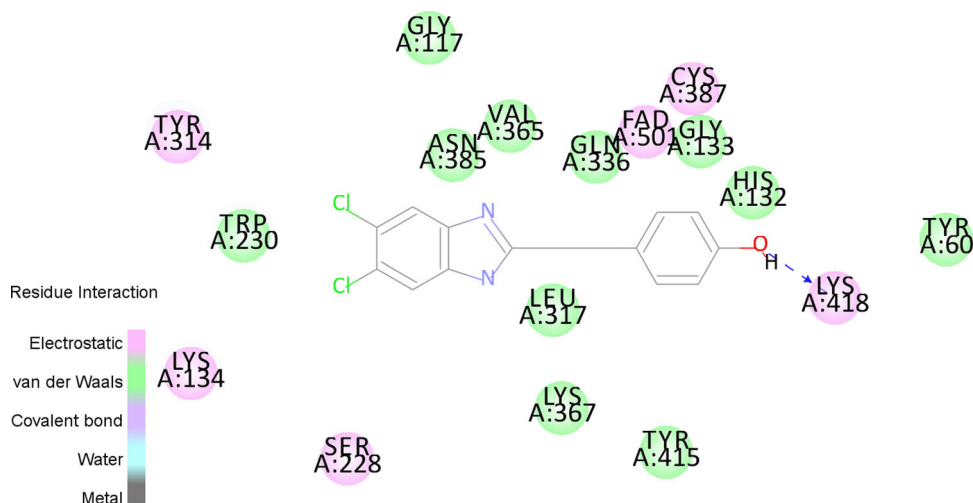


Figure 13. CDOCKER docking profile of 21. Blue discrete dots between LYS418 and the hydroxyl group of benzimidazole ring show the H bond.

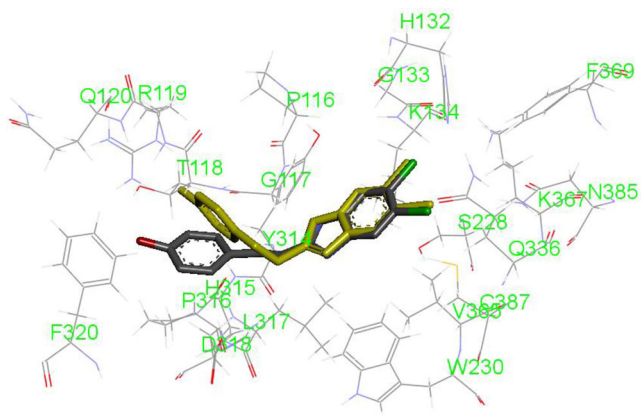


Figure 14. Superposition of dock results of CDOCKER and Autodock Vina. Yellow 21 demonstrates the result of AutoDock Vina (Figure was taken by AutoDock Vina).

molecules still used in the treatment of TB, some mutant MTB strains have been found to show drug resistance in the presence of these molecules (Aggarwal et al., 2017). 23 new benzimidazole and bisbenzimidazole derivatives were therefore

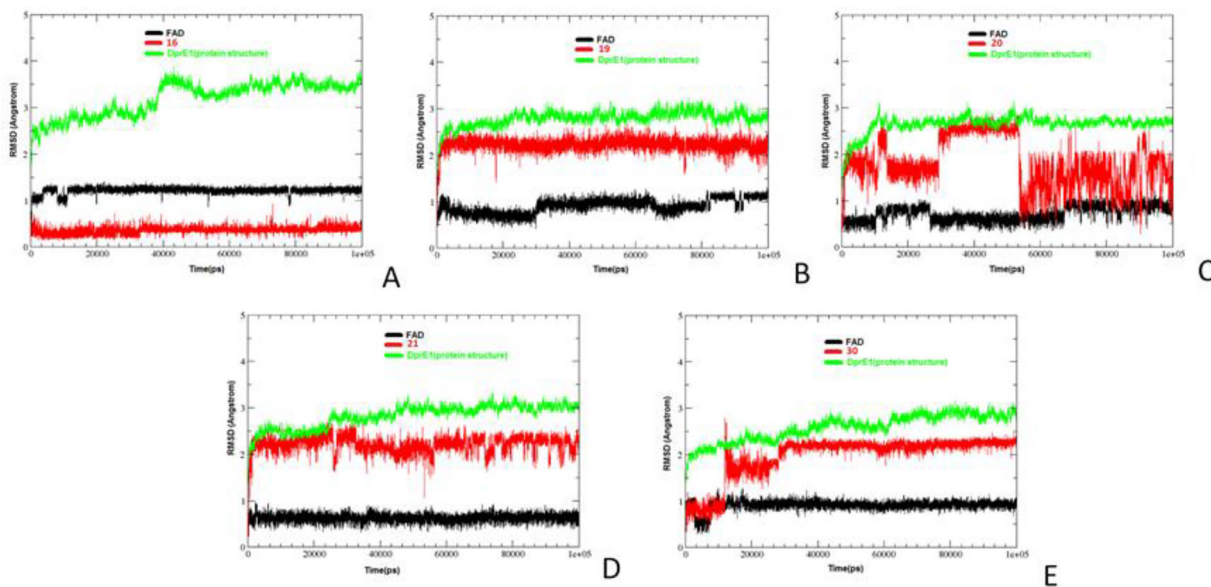
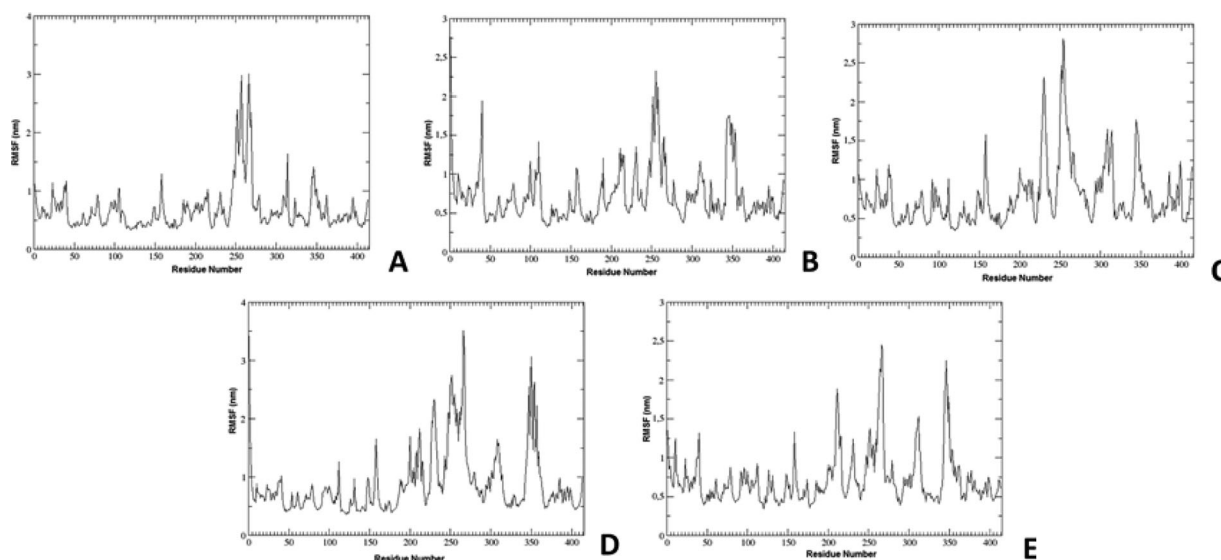
investigated for their antitubercular activity. Compounds **20**, **21**, and **30** show significant activities and other compounds exhibit moderate activities. This indicates that two-atom linker compounds appear to enhance the inhibition activity of the molecules. The presence of chloro groups on the phenyl of benzimidazole increases antitubercular activity and activity decreases in the presence of methyl groups on the same ring.

Docking was used to explain protein-ligand interactions through computational prediction. This prediction demonstrates how similar the ligand binding prediction is to ligand conformation determined experimentally (Ansari et al., 2018). A scoring method has been used for this purpose and the ligands were ranked based on this. Different results obtained by using different programs and methods could cause computational studies to be unreliable.

In the context of inverse docking studies, the interaction of ligands with 4 proteins (EmbC, FtsZ, PtpB, DprE1) was screened, and the interaction of compounds with DprE1 was found to be higher. The interaction of 3 proteins (EmbC, FtsZ, PtpB) with X-ray ligands were compared with the

TABLE 9. Comparison of two docking programs for best benzimidazole derivatives.

Compound	Autodock Vina		CDOCKER	
	Residues	H-Bond Distance (Å)	Residues	H-Bond Distance (Å)
21	SER228, LYS134	1.89, 3.94	LYS418	1.76
30	SER228, LYS134, TYR314	2.89, 3.94, 1.98	HIS132	1.71

**Figure 15.** Root mean square deviation (RMSD) curves for all systems. (A) 16-FAD-DprE1 complex. (B) 19-FAD-DprE1 complex. (C) 20-FAD-DprE1 complex. (D) 21-FAD-DprE1 complex. (E) 30-FAD-DprE1 complex.**Figure 16.** RMSF curves for all systems. (A) 16-FAD-DprE1 complex. (B) 19-FAD-DprE1 complex. (C) 20-FAD-DprE1 complex. (D) 21-FAD-DprE1 complex. (E) 30-FAD-DprE1 complex.

interaction of compounds (Figures 3 and 4). While the X-ray ligands were observed to be packed with the binding package with dense hydrogen bonds, the same binding profile was not observed with the compounds in Table 1. However, the interaction of the compounds with DprE1 was similar to the interaction with the X-ray ligand (O95).

The binding pocket (Panda et al., 2014) and the crystal structure of DprE1 with FAD and **O95** molecule (Grundner et al., 2007) were proven in the literature. The docking similarity between AutoDock Vina and CDOCKER was examined

on derivatives with the best results. These results are shown in Table 7. Two docking modules generate H bonds with different residues and the reason how these ligands are kept in a binding pocket is shown.

AutoDock Vina uses a global heuristic optimizer algorithm, iterated local search, with a local optimization algorithm called Broyed–Fletcher–Goldfarb–Shanno (BFGS). Stochastic algorithms provide the flexibility of the complete model for both the ligand and the receptor. However, there are concerns about reaching convergence because of the method's

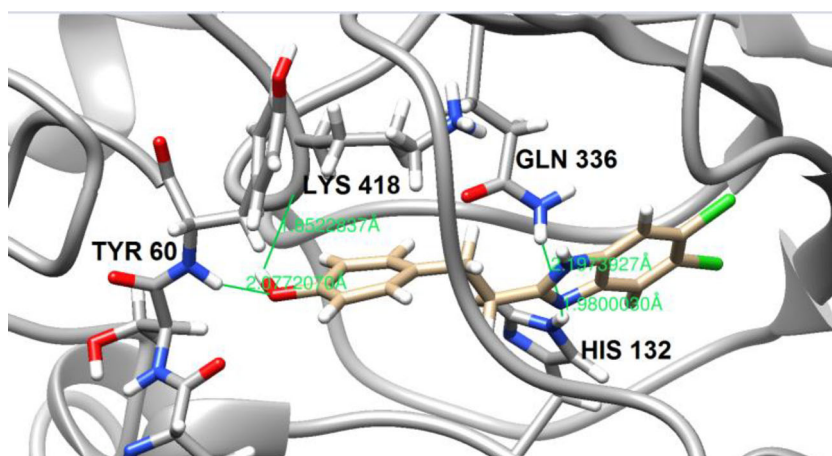


Figure 17. Compound 21 is surrounded by hydrogen bonds with TYR60 (2.07 Å), LYS418 (1.85 Å), HIS132 (1.98 Å), GLN336 (2.19 Å) at the end of the MD simulation. The simulation's binding profile is given in the [Supplementary Video S1](#) for 100 ns.

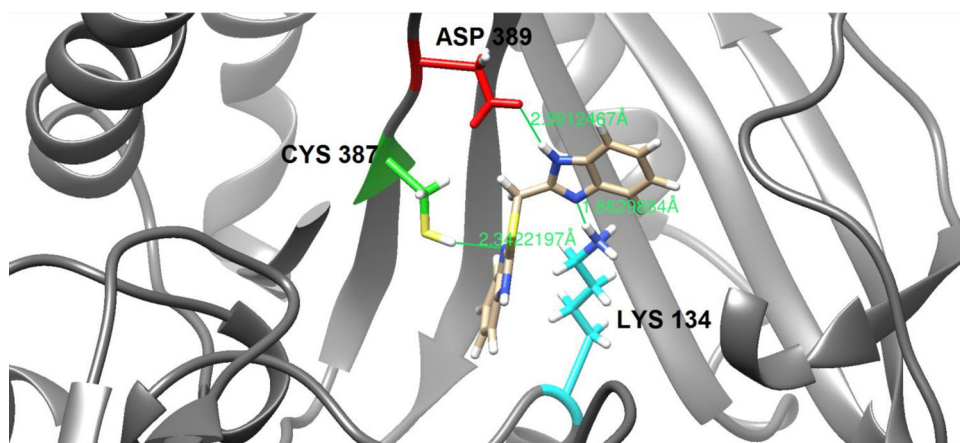


Figure 18. Compound 30 is surrounded by hydrogen bonds with CYS387 (2.34 Å), LYS134 (2.34 Å), and ASP389 (2.39 Å) at the end of the MD simulation. The binding profile of the simulation is given in the [Supplementary Video S2](#) for 100 ns.

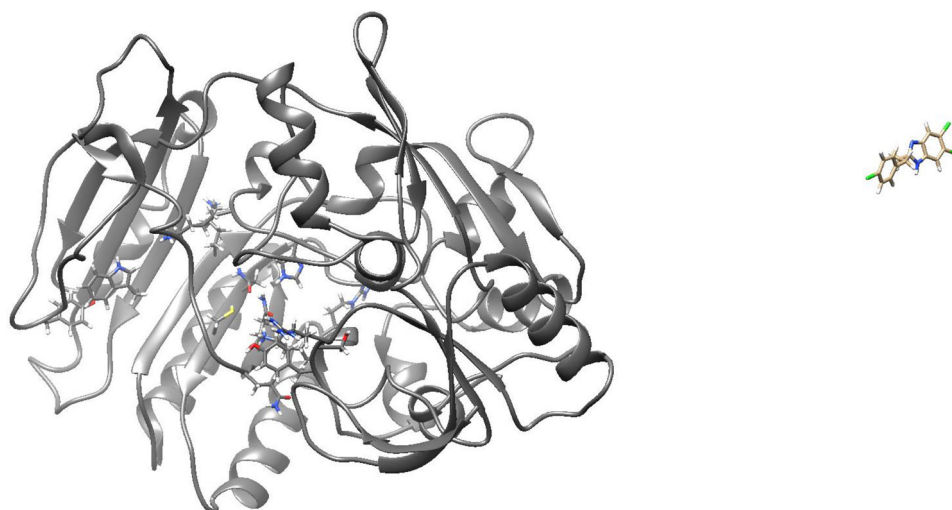


Figure 19. Compound 20 is seen away from the receptor at the end of the MD simulation. The binding profile of the simulation is given in the [Supplementary Video S3](#) for 100 ns.

random numbering. Because of this, the method requires multiple independent docking runs (Spyrakis et al., 2016).

CDOCKER was a semiflexible docking program based on MD. The conformation on the receptor's active site was optimized, whereas the flexible conformation of the ligand was searched (Spyrakis et al., 2016). However, although both

methods gave similar results, CDOCKER was found to be more reliable than AutoDock Vina (Bai et al., 2014).

While simulations were examined, only compounds **21** and **30** were found to be on binding pocket after 100 ns because of their strong H bonds with the residues (LYS 418, GLN 336, TYR 60, HIS 132, ASN 389, CYS 387, and LYS 134).

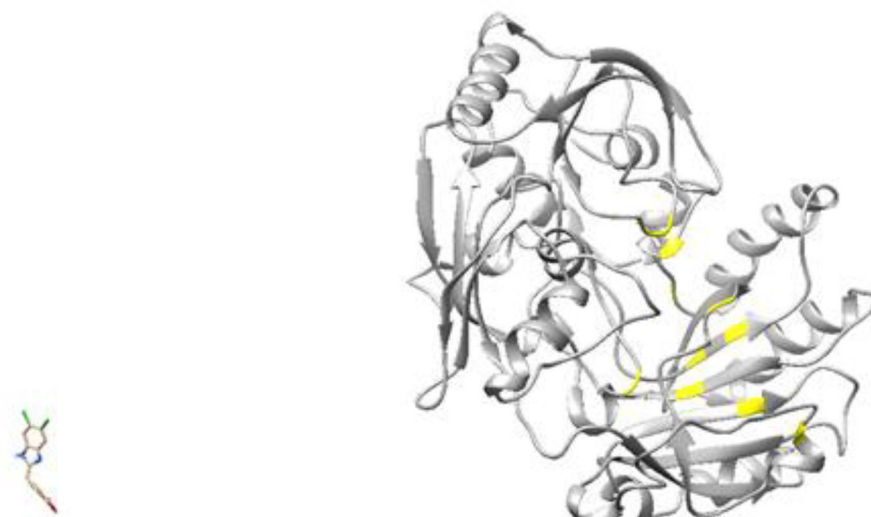


Figure 20. Compound **16** is seen away from the receptor at the end of the MD simulation. The binding profile of the simulation is given in the [Supplementary Video S4](#) for 100 ns.

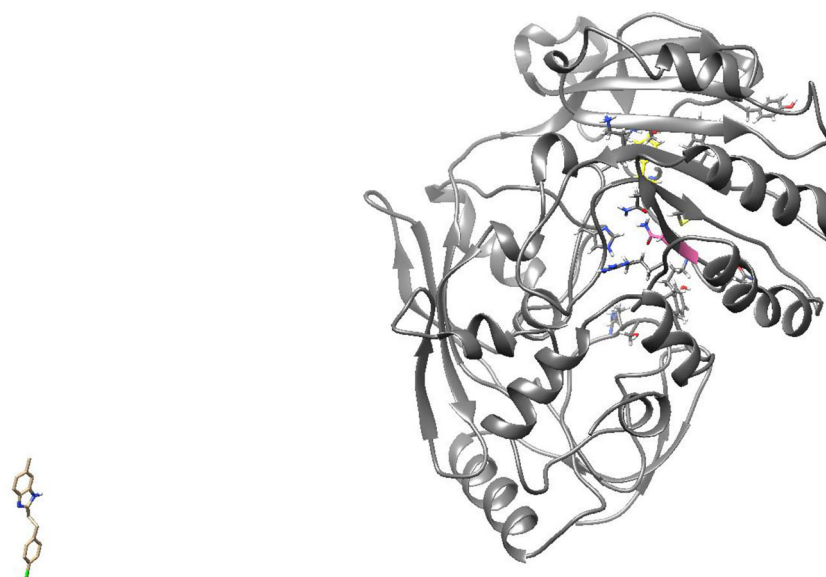


Figure 21. Compound **19** can be seen away from the receptor at the end of the MD simulation. The binding profile of the simulation is given in the [Supplementary Video S5](#) for 100 ns.

The holding of these ligands on the binding pocket demonstrates that they could be possible drug leads for the DprE1 protein.

When the relationship of ligand-protein interactions with the antitubercular effect was examined, it was observed that the NH of the benzimidazole ring was quite important in accordance with the literature. On the other hand, unlike benzimidazole compounds in other literature, the hydroxyl group of the benzene ring was found to be quite active. The key residue in the literature is LYS418 (Lipinski, 2004; Stanley et al., 2012; Warriar et al., 2016). It has been observed that the NH structure of LYS, which forms the basis for both hydrogen bonds and π interactions, also bonds to a large extent with benzimidazole derivatives in our study (Lipinski, 2004). In addition, TYR 60, HIS132, TYR314 and GLN336 residues, which are effective in antitubercular drugs in the literature, have also been found to interact with our compounds

(Lipinski, 2004). Finally, it has been clearly shown in the literature that the benzimidazole ring and the aromatic structure of the TRP230 residue perform π - π interaction. The same interaction was observed in our compounds. As a result, it can be said that the structure of compounds **30** and **21** may lead to antitubercular effects in parallel with the literature.

For the approximation of the calculated results to experimental results, one of the most important things for MD simulations is the choice of solvent. The implicit method does not require the explicit calculation of a large number of individual interactions between atoms of individual solvent molecules. However, explicit solvent implementation was found more accurate than the implicit solvent approach (Anandakrishnan et al., 2015), which is that used in molecular simulations. Because of this reason, the explicit solvent method was used for the solution of our MD systems.

ADME-toxicology analyses are important in understanding the druggability of ligands. To reduce the number of synthesized compounds with inadequate ADME properties, *in silico* ADME studies are provided. *In silico* modeling was implemented in determining the ligand with good physicochemical features. Catalyst (Accelrys Software Inc, 2012) that was used for *in silico* ADME studies was found to outperform the other program packages (Yamashita & Hashida, 2004).

In terms of absorption in the human intestinal tract, compounds **16**, **19**, **21**, and most of group 5 are in the acceptable range. At the same time, although the logP values of these molecules were found to be following the Lipinski rules, it was determined that the molecule with the lowest lipophilicity was 12. This means that compounds **12**, **16**, **19**, **21**, and most of group 5 could be used as candidates in developing new drugs.

5. Conclusion

The new drug approach is to produce fast and efficient drugs with less toxic properties and less acute side effects (Yuan et al., 2019). Currently, the conventional approach of drug discovery, replaced by the rational approach of the computer-aided drug design process, has evolved and plays a significant contribution in the computation and retrieval of hit compounds from vast compound databases (Mahajan et al., 2020). One of the popular discussion topics of computational chemistry is what the most reliable docking program and method are. Recent studies give different answers to this question. Molecular docking is becoming important for drug design studies. Bai et al. reported that CDOCKER had the most reliable results in their work (Bai et al., 2014). On the other hand, Ahn et al. (2018) found the same rankings of three molecules (troglitazone, 2-formyl-komarovicine, and komarovicine) in both programs.

Another issue to be considered in the docking methodology is the rigidity of the receptor. Many docking software have been compared in the literature. It has been stated that all flexible docking programs except GOLD keep the protein structure rigid. In the same study, many docking programs (DOCK, AutoDock, FlexX, Surflex, GOLD, ICM, Glide, Cdocker, LigandFit, MCDock, FRED, MOE-Dock, LeDock, AutoDock Vina, rDock, UCSF Dock) were examined, and it was observed that AutoDock Vina, GOLD, and MOE-Dock predicted the top poses with the best scores (Pagadala et al., 2017; Ravindranath et al., 2015). In this respect, it is not correct to reach a definite conclusion that the rigidity of the receptor affects the docking results.

In line with Ahn's study (Ahn et al., 2018), we have chosen the combination of the two methods to predict the best molecule for DprE1 enzyme's inhibition.

Some novel antimycobacterial lead molecules with attractive microbiological properties have been established in this study. Then molecular docking and molecular dynamic studies were realized with 23 molecules, which include the benzimidazole nucleus. Extensive antitubercular susceptibility tests and *in silico* studies such as molecular docking, binding affinity, and pharmacokinetics profile filtering results in the

selection of three compounds **20**, **21**, and **30**, which explored potential drug candidates were conducted. Although the MIC values of these molecules (3.90 µg/mL, 7.81 µg/mL, 3.90 µg/mL, respectively) have been determined to be less than half of the known drug molecules (INH (0.97 µg/mL), EMB (1.95 µg/mL)), molecular docking studies demonstrate the molecules exhibited less than -8.0 kcal/mol binding affinity values. Best-docked results were detected with **20** and **21** from the 2nd group and **30**. Either imidazole NH or pyridine N atoms of benzimidazole ring were found to be the most important groups for binding into DprE1. The second benzimidazole group was not found to be impressive on binding affinity score and binding profile. SER 228, GLN 336, GLN 334, ASN 385, TYR 314, TRP 230, LYS 134, HIS 132, LYS 418, TYR 60 residues, which are in the binding pocket of DprE1, were found to be interacting with lead molecules, which is consistent with the literature (Genheden et al., 2010). Compound **21** was found to be the best molecule with its binding affinity value. This result was also supported with *in silico* ADME modeling and MD simulations.

It has been stated in the literature that the DprE1 enzyme is also an important target to overcome the drug resistance in MTB (Foo et al., 2016; Gawad & Bonde, 2018). Results indicated that the screened compounds possess a desirable binding affinity to the DprE1 receptor. Identification of the novel therapeutic scaffolds will help researchers design enhanced inhibitors with maximum possible side effects.

Based on advanced molecular modelling data, we have then reconstructed the overall properties of the benzimidazole structure for DprE1 inhibitors and showed that it has a compact structure. Our data represent an important step toward the structural characterization of the properties of benzimidazole derivatives and their DprE1 inhibitor activities.

Disclosure statement

No potential conflict of interest was reported by the authors.

Funding

We gratefully acknowledge the financial support from Mersin University (BAP, No: 2015-AP3-1320). The numerical calculations reported in this paper were fully/partially performed at TUBITAK ULAKBIM, High Performance and Grid Computing Center (TRUBA resources).

ORCID

Gozde Yalcin-Ozkat  <http://orcid.org/0000-0002-9689-2239>
Serdar Burmaoglu  <http://orcid.org/0000-0001-8288-7423>
Ilkay Yildiz  <http://orcid.org/0000-0001-9526-0232>
Oztekin Algul  <http://orcid.org/0000-0001-5685-7511>

References

- Accelrys Software Inc. (2012). *Discovery studio 3.5 client*. Accelrys Inc.
- Advanced Chemistry Development Inc. (2001). ACD/ChemSketch.
- Afriza, D., Suriyah, W. H., & Ichwan, S. J. A. (2018). In silico analysis of molecular interactions between the anti-apoptotic protein survivin and dentatin, nordentatin, and quercetin. *Journal of Physics:*

- Conference Series*, 1073(3), 032001. <https://doi.org/10.1088/1742-6596/1073/3/032001>.
- Aggarwal, A., Parai, M. K., Shetty, N., Wallis, D., Woolhiser, L., Hastings, C., Dutta, N. K., Galaviz, S., Dhakal, R. C., Shrestha, R., Wakabayashi, S., Walpole, C., Matthews, D., Floyd, D., Scullion, P., Riley, J., Epemolu, O., Norval, S., Snively, T., ... Sacchettini, J. C. (2017). Development of a novel lead that targets m. tuberculosis polyketide synthase 13. *Cell*, 170(2), 249–259.e25. <https://doi.org/10.1016/j.cell.2017.06.025>
- Ahn, S., Lee, M., An, S., Hyun, S., Hwang, J., Lee, J., & Noh, M. (2018). 2-Formyl-komarovicine promotes adiponectin production in human mesenchymal stem cells through PPAR γ partial agonism. *Bioorganic & Medicinal Chemistry*, 26(5), 1069–1075. <https://doi.org/10.1016/j.bmc.2018.01.019>
- Akinpelu, O. I., Lawal, M. M., Kumalo, H. M., & Mhlongo, N. N. (2020a). Computational studies of the properties and activities of selected tri-substituted benzimidazoles as potential antitubercular drugs inhibiting MTB-FtsZ polymerization. *Journal of Biomolecular Structure and Dynamics*, 1–13. <https://doi.org/10.1080/07391102.2020.1830176>
- Akinpelu, I. O., Monsurat, M. L., Hezekiel, M. K., & Ndumiso, N. M. (2020b). Drug repurposing: Fusidic acid as a potential inhibitor of M. tuberculosis FtsZ polymerization – Insight from DFT calculations, molecular docking and molecular dynamics simulations. *Tuberculosis (Edinburgh, Scotland)*, 121, 101920. <https://doi.org/10.1016/j.tube.2020.101920>
- Akpa, S. J., Say, M. V., Zoakouma, R. S. P., Fanté, B., Sissouma, D., & Adjou, A. (2016). Synthesis of 2-(benzylthio)benzimidazole, 2-[(benzimidazol-2-yl)methylthio]benzimidazole and structural analogues against *Haemoncus contortus*, Afr. *Journal of Pharmacy and Pharmacology*, 10, 670–680. <https://doi.org/10.5897/AJPP2016.4557>
- Alderwick, L. J., Lloyd, G. S., Ghadbane, H., May, J. W., Bhatt, A., Eggeling, L., Fütterer, K., & Besra, G. S. (2011). The C-terminal domain of the arabinosyltransferase mycobacterium tuberculosis EmbC is a lectin-like carbohydrate binding module. *PLoS Pathogens*, 7(2), e1001299. <https://doi.org/10.1371/journal.ppat.1001299>
- Anandakrishnan, R., Drozdetski, A., Walker, R. C., & Onufriev, A. V. (2015). Speed of conformational change: Comparing explicit and implicit solvent molecular dynamics simulations. *Biophysical Journal*, 108(5), 1153–1164. <https://doi.org/10.1016/j.bpj.2014.12.047>
- Ansari, S. A., Jafri, M. A., Satar, R., Ahmad, S. I., & Chibber, S. (2018). Molecular docking as a computational tool for analyzing product mediated inhibition for β -galactosidase immobilized on glutaraldehyde modified matrices. *Oriental Journal of Chemistry*, 34(2), 820–824. <https://doi.org/10.13005/ojc/340227>
- Ayaz, F., Ersan, R. H., Kuzu, B., & Algul, O. (2020). New-generation benzimidazole-based plasmid delivery reagents with high transfection efficiencies on the mammalian cells. *In Vitro Cellular & Developmental Biology. Animal*, 56(1), 34–41. <https://doi.org/10.1007/s11626-019-00418-4>
- Bai, Q., Shao, Y., Pan, D., Zhang, Y., Liu, H., & Yao, X. (2014). Search for β_2 adrenergic receptor ligands by virtual screening via grid computing and investigation of binding modes by docking and molecular dynamics simulations. *PLoS One*, 9(9), e107837. <https://doi.org/10.1371/journal.pone.0107837>
- Batt, S. M., Jabeen, T., Bhowruth, V., Quill, L., Lund, P. A., Eggeling, L., Alderwick, L. J., Fütterer, K., & Besra, G. S. (2012). Structural basis of inhibition of Mycobacterium tuberculosis DprE1 by benzothiazinone inhibitors. *Proceedings of the National Academy of Sciences of the United States of America*, 109(28), 11354–11359. <https://doi.org/10.1073/pnas.1205735109>
- Boggu, P. R., Venkateswararao, E., Manickam, M., Kwak, D., Kim, Y., & Jung, S. (2016). Exploration of 2-benzylbenzimidazole scaffold as novel inhibitor of NF- κ B. *Bioorganic & Medicinal Chemistry*, 24(8), 1872–1878. <https://doi.org/10.1016/j.bmc.2016.03.012>
- Burmaoglu, S., Algul, O., Gobek, A., Aktas Anil, D., Ulger, M., Erturk, B. G., Kaplan, E., Dogen, A., & Aslan, G. (2017). Design of potent fluoro-substituted chalcones as antimicrobial agents. *Journal of Enzyme Inhibition and Medicinal Chemistry*, 32(1), 490–495. <https://doi.org/10.1080/14756366.2016.1265517>
- Carugo, O., & Pongor, S. (2001). A Normalized root-mean-square distance for comparing protein three-dimensional structures. *Protein Science: A Publication of the Protein Society*, 10(7), 1470–1473. doi: 10.1110/ps.690101.)
- Case, D. A., Babin, V., Berryman, J. T., Betz, R. M., Cai, Q., Cerutti, D. S., Cheatham, T. E., Darden, T. A., Duke, R. E., Gohlke, H., Goetz, A. W., Gusarov, S., Homeyer, N., Janowski, P., Kaus, J., Kolossváry, I., Kovalenko, A., Lee, T. S., LeGrand, S. ... Kollman, P. A. (2014). *AMBER 14*. University of California.
- Clinical and Laboratory Standards Institute (CLSI) (formerly NCCLS). (2002). Antimycobacterial susceptibility testing for M. tuberculosis: Tentative standard NCCLS document M24-T, Villanova, Pennsylvania.
- Djemoui, A., Naouri, A., Ouahrani, M. R., Djemoui, D., Lahcene, S., Lahrech, M. B., Boukenna, L., Albuquerque, H. M. T., Saher, L., Rocha, D. H. A., Monteiro, F. L., Helguero, L. A., Bachari, K., Talhi, O., & Silva, A. M. S. (2020). A step-by-step synthesis of triazole-benzimidazole-chalcone hybrids: Anticancer activity in human cells⁺. *Journal of Molecular Structure*, 1204, 127487. <https://doi.org/10.1016/j.molstruc.2019.127487>
- Duran, G. G., Küçük, M. U., Algül, Ö., & Terzi, M. Y. (2020). Investigation of new benzimidazole derivative compounds' effects on A549 cell line. *Brazilian Archives of Biology and Technology*, 63, e20190364. <https://doi.org/10.1590/1678-4324-2020190364>
- Ersan, R. H., Alagoz, M. A., Ertan-Bolelli, T., Duran, N., Burmaoglu, S., & Algul, O. (2020). Head-to-head bisbenzazole derivatives as antiproliferative agents: Design, synthesis, in vitro activity, and SAR analysis. *Mol. Divers.* 25(4), 2247–2259. <https://doi.org/10.1007/s11030-020-10115-0>
- Ersan, R. H., Yuksel, A., Ertan-Bolelli, T., Dogen, A., Burmaoglu, S., & Algul, O. (2021). One-pot synthesis of novel benzimidazoles with a naphthalene moiety as antimicrobial agents and molecular docking studies. *Journal of the Chinese Chemical Society*, 68(2), 374–383. <https://doi.org/10.1002/jccs.202000125>
- Foo, C. S., Lechartier, B., Kolly, G. S., Boy-Röttger, S., Neres, J., Rybniker, J., Lupien, A., Sala, C., Piton, J., & Cole, S. T. (2016). Characterization of DprE1-mediated benzothiazinone resistance in mycobacterium tuberculosis. *Antimicrobial Agents and Chemotherapy*, 60(11), 6451–6459. <https://doi.org/10.1128/AAC.01523-16>
- Gawad, J., & Bonde, C. (2018). Decaprenyl-phosphoryl-ribose 2'-epimerase (DprE1): Challenging target for antitubercular drug discovery. *Chemistry Central Journal*, 12(1), 72. <https://doi.org/10.1186/s13065-018-0441-2>
- Genheden, S., Luchko, T., Gusarov, S., Kovalenko, A., & Ryde, U. (2010). An MM/3D-RISM Approach for Ligand Binding Affinities. *The Journal of Physical Chemistry. B*, 114(25), 8505–8516. <https://doi.org/10.1021/jp101461s>
- Götz, A. W., Williamson, M. J., Xu, D., Poole, D., Le Grand, S., & Walker, R. C. (2012). Routine microsecond molecular dynamics simulations with AMBER on GPUs. 1. Generalized Born. *Journal of Chemical Theory and Computation*, 8(5), 1542–1555. <https://doi.org/10.1021/ct200909j>
- Gozelle, M., Süloğlu, A. K., Selmanoğlu, G., Ramazanoğlu, N., Açıık, L., & Gümüş, F. (2019). Studies on the synthesis, characterization, cytotoxic activities and plasmid DNA binding of platinum(II) complexes having 2-substituted benzimidazole ligands. *Polyhedron*, 161, 298–308. <https://doi.org/10.1016/j.poly.2019.01.028>
- Grundner, C., Perrin, D., van Huijsduijnen, R. H., Swinnen, D., Gonzalez, J., Gee, C. L., Wells, T. N., & Alber, T. (2007). Structural basis for selective inhibition of mycobacterium tuberculosis protein tyrosine phosphatase PtpB. *Structure (London, England : 1993)*, 15(4), 499–509. <https://doi.org/10.1016/j.str.2007.03.003>
- Gümüş, F., Altuntas, T. G., Saygun, N., Ozden, T., & Ozden, S. (1989). In vitro tuberculostatic activities of some 2-benzylbenzimidazole and 2-phenoxymethylbenzimidazole derivatives. *Journal de Pharmacie de Belgique*, 44(6), 398–402.
- Hall, L., Jude, K. P., Clark, S. L., & Wengenack, N. L. (2011). Antimicrobial susceptibility testing of Mycobacterium tuberculosis complex for first and second line drugs by broth dilution in a microtiter plate format. *Journal of Visualized Experiments*, 52, 3094. <https://doi.org/10.3791/3094>
- Harding, E. (2020). WHO global progress report on tuberculosis elimination. *The Lancet Respiratory Medicine*, 8(1), 19. [https://doi.org/10.1016/S2213-2600\(19\)30418-7](https://doi.org/10.1016/S2213-2600(19)30418-7)
- <https://www.who.int/publications/i/item/global-tuberculosis-report-2019>.

- Kopel, P., Wawrzak, D., Langer, V., Cihalova, K., Chudobova, D., Vesely, R., Adam, V., & Kizek, R. (2015). Biological activity and molecular structures of bis(benzimidazole) and trithiocyanurate complexes. *Molecules (Basel, Switzerland)*, 20(6), 10360–10376. <https://doi.org/10.3390/molecules200610360>
- Kumari, R., Kumar, R., & Lynn, A. (2014). g_mmpbsa-A GROMACS tool for high-throughput MM-PBSA calculations. *Journal of Chemical Information and Modeling*, 54(7), 1951–1962. <https://doi.org/10.1021/ci500020m>
- Leung, A. K. W., White, E. L., Ross, L. J., Reynolds, R. C., Devito, J. A., & Borhani, D. W. (2004). Structure of mycobacterium tuberculosis FtsZ reveals unexpected, G protein-like conformational switches. *Journal of Molecular Biology*, 342(3), 953–970. <https://doi.org/10.1016/j.jmb.2004.07.061>
- Lipinski, C. A. (2004). Lead- and drug-like compounds: The rule-of-five revolution. *Drug Discovery Today. Technologies*, 1(4), 337–341. <https://doi.org/10.1016/j.ddtec.2004.11.007>
- Mahajan, P., Wadhwa, B., Barik, M. R., Malik, F., & Nargotra, A. (2020). Combining ligand- and structure-based in silico methods for the identification of natural product-based inhibitors of Akt1. *Molecular Diversity*, 24(1), 45–60. <https://doi.org/10.1007/s11030-019-09924-9>
- Maharaj, Y., Bhakat, S., & Soliman, M. (2015). Computer-aided identification of novel DprE1 inhibitors as potential anti-TB lead compounds: A hybrid virtual-screening and molecular dynamics approach. *Letters in Drug Design & Discovery*, 12(4), 302–313. <https://doi.org/10.2174/1570180811666141001005536>
- Maia, M. S., de Sousa, N. F., Rodrigues, G. C. S., Monteiro, A. F. M., Scotti, M. T., & Scotti, L. (2020). Lignans and neolignans anti-tuberculosis identified by QSAR and molecular modeling. *Combinatorial Chemistry & High Throughput Screening*, 23(6), 504–516. <https://doi.org/10.2174/1386207323666200226094940>
- Maier, J. A., Martinez, C., Kasavajhala, K., Wickstrom, L., Hauser, K. E., & Simmerling, C. (2015). ff14SB: Improving the accuracy of protein side chain and backbone parameters from ff99SB. *Journal of Chemical Theory and Computation*, 11(8), 3696–3713. <https://doi.org/10.1021/acs.jctc.5b00255>
- Makarov, V., Manina, G., Mikusova, K., Möllmann, U., Ryabova, O., Saint-Joanis, B., Dhar, N., Pasca, M. R., Bironi, S., Lucarelli, A. P., Milano, A., De Rossi, E., Belanova, M., Bobovska, A., Dianiskova, P., Kordulakova, J., Sala, C., Fullam, E., Schneider, P., ... Cole, S. T. (2009). Benzothiazinones Kill Mycobacterium tuberculosis by Blocking Arabinan Synthesis. *Science (New York, N.Y.)*, 324(5928), 801–804. <https://doi.org/10.1126/science.1171583>
- Manjunatha, M. R., Randa, S., Manoranjan, P., Clair, S., Anisha, A., Vijender, P., Naveen, K., Jyothi, M., Sreenivasaiah, M., Narayan, A., Supreeth, G., Sreevalli, S., Vasana, K. S., Vasanthi, R., Meenakshi, M., Cooper, C., Khisi, M., Scott, B., Ruben, T., ... Shirude, P. S. (2019). Scaffold morphing to identify novel DprE1 inhibitors with antimycobacterial activity. *ACS Medicinal Chemistry Letters*, 10(10), 1480–1485. <https://doi.org/10.1021/acsmchemlett.9b00343>
- National Committee for Clinical Laboratory Standards. (2003). Susceptibility testing of mycobacteria, nocardia, and other aerobic actinomycetes: Approved standard NCCLS document M24-A, Wayne, Pennsylvania.
- Neres, J., & Cole, S. T. (2016). Non-mutagenic nitrobenzothiazoles as novel anti-tubercular agents: A balance between potency and electron affinity. <https://doi.org/10.2210/pdb4p8h/pdb>
- Nguyen, N. T., Nguyen, T. H., Han Pham, T. N., Huy, N. T., Bay, M. V., Pham, M. Q., Nam, P. C., Vu, V. V., & Ngo, S. T. (2020). Autodock vina adopts more accurate binding poses but autodock4 forms better binding affinity. *Journal of Chemical Information and Modeling*, 60(1), 204–211. doi: 10.1021/acs.jcim.9b00778.
- Niknam, K., & Fatehi-Raviz, A. (2007). Synthesis of 2-substituted benzimidazoles and bis-benzimidazoles by microwave in the presence of alumina-methanesulfonic acid. *Journal of the Iranian Chemical Society*, 4(4), 438–443. <https://doi.org/10.1007/BF03247230>
- Nisha, D., Kumar Jena, P., & Kumar Pradhan, S. (2020). Arabinosyltransferase C enzyme of mycobacterium tuberculosis, a potential drug target: An insight from molecular docking study. *Heliyon*, 6(2), e02693. doi: 10.1016/j.heliyon.2019.e02693.
- Oren, I., Temiz, O., Yalcin, I., Sener, E., Akin, A., & Uçartürk, N. (1997). Synthesis and microbiological activity of 5 (or 6)-methyl-2-substituted benzoxazole and benzimidazole derivatives. *Arzneimittel-Forschung*, 47(12), 1393–1397.
- Pagadala, N. S., Syed, K., & Tuszyński, J. (2017). Software for molecular docking: A review. *Biophysical Reviews*, 9(2), 91–102. <https://doi.org/10.1007/s12551-016-0247-1>
- Panda, M., Ramachandran, S., Ramachandran, V., Shirude, P. S., Humnabadkar, V., Nagalapur, K., Sharma, S., Kaur, P., Guptha, S., Narayan, A., Mahadevaswamy, J., Ambady, A., Hegde, N., Rudrapatna, S. S., Hosagrahara, V. P., Sambandamurthy, V. K., & Raichurkar, A. (2014). Discovery of pyrazolopyridones as a novel class of noncovalent DprE1 inhibitor with potent anti-mycobacterial activity. *Journal of Medicinal Chemistry*, 57(11), 4761–4771. <https://doi.org/10.1021/jm5002937>
- Pettersen, E. F., Goddard, T. D., Huang, C. C., Couch, G. S., Greenblatt, D. M., Meng, E. C., & Ferrin, T. E. (2004). UCSF Chimera—a visualization system for exploratory research and analysis. *Journal of Computational Chemistry*, 25(13), 1605–1612. <https://doi.org/10.1002/jcc.20084>
- Phillips, M. A. (1928). The formation of 2-substituted benzimidazoles. *Journal of the Chemical Society.*, 1928, 2393–2399. <https://doi.org/10.1039/JR9280002393>
- Prakash, A., & Luthra, P. M. (2012). Insilico study of the A(2A)R-D (2R) kinetics and interfacial contact surface for heteromerization. *Amino Acids*, 43(4), 1451–1464. <https://doi.org/10.1007/s00726-012-1218-x>
- Ravindranath, P. A., Forli, S., Goodsell, D. S., Olson, A. J., & Sanner, M. F. (2015). AutoDockFR: Advances in protein-ligand docking with explicitly specified binding site flexibility. *PLoS Computational Biology*, 11(12), e1004586. <https://doi.org/10.1371/journal.pcbi.1004586>
- Riccardi, G., Pasca, M. R., Chiarelli, L. R., Manina, G., Mattevi, A., & Binda, C. (2013). The DprE1 enzyme, one of the most vulnerable targets of *Mycobacterium tuberculosis*. *Applied Microbiology and Biotechnology*, 97(20), 8841–8848. <https://doi.org/10.1007/s00253-013-5218-x>
- Salomon-Ferrer, R., Götz, A. W., Poole, D., Le Grand, S., & Walker, R. C. (2013). Routine microsecond molecular dynamics simulations with AMBER on GPUs. 2. Explicit Solvent Particle Mesh Ewald. *Journal of Chemical Theory and Computation*, 9(9), 3878–3888. <https://doi.org/10.1021/ct400314y>
- Sarkar, P., Yarlagadda, V., Ghosh, C., & Haldar, J. (2017). A review on cell wall synthesis inhibitors with an emphasis on glycopeptide antibiotics. *MedChemComm*, 8(3), 516–533. doi: 10.1039/c6md00585c.
- Sastry, G. M., Adzhigirey, M., Day, T., Annabhimoju, R., & Sherman, W. (2013). Protein and ligand preparation: Parameters, protocols, and influence on virtual screening enrichments. *Journal of Computer-Aided Molecular Design*, 27(3), 221–234. <https://doi.org/10.1007/s10822-013-9644-8>
- Sayed, A. M., Alhadrami, H. A., El-Hawary, S. S., Mohammed, R., Hassan, H. M., Rateb, M. E., Abdelmohsen, U. R., & Baker, W. (2020). Discovery of two brominated oxindole alkaloids as staphylococcal DNA gyrase and pyruvate kinase inhibitors via inverse virtual screening. *Microorganisms*, 8(2), 293. <https://doi.org/10.3390/microorganisms8020293>
- Singh, S., Kumar Srivastava, H., Kishor, G., Singh, H., Agrawal, P., & Raghava, G. P. S. (2017). Evaluation of protein-ligand docking methods on peptide-ligand complexes for docking small ligands to peptides. *BioRxiv*, 212514. <https://doi.org/10.1101/212514>
- Sparks, R. B., Polam, P., Zhu, W., Crawley, M. L., Takvorian, A., McLaughlin, E., Wei, M., Ala, P. J., Gonnevillie, L., Taylor, N., Li, Y., Wynn, R., Burn, T. C., Liu, P. C. C., & Combs, A. P. (2007). Benzothiazole benzimidazole (S)-isothiazolidinone derivatives as protein tyrosine phosphatase-1B inhibitors. *Bioorganic & Medicinal Chemistry Letters*, 17(3), 736–740. <https://doi.org/10.1016/j.bmcl.2006.10.079>
- Spyrakakis, F., Cozzini, P., & Kellogg, G. E. (2016). Applying computational scoring functions to assess biomolecular interactions in food science: Applications to the estrogen receptors. *NuRR*, 3, 1–21. <https://doi.org/10.11131/2016/101202>
- Stanley, S. A., Grant, S. S., Kawate, T., Iwase, N., Shimizu, M., Wivagg, C., Melanie, S., Kazysanskaya, E., Aquadro, J., Golas, A., Fitzgerald, M., Dai, H., Zhang, L., & Hung, D. T. (2012). Identification of novel inhibitors of

- M. tuberculosis growth using whole cell based high-throughput screening. *ACS Chemical Biology*, 7(8), 1377–1384. doi: [10.1021/acsmchemlett.9b00343](https://doi.org/10.1021/acsmchemlett.9b00343)
- Thanh, N. D., Do, H. S., Nguyen, T. T. H., Do, T. T., Cao, T. L., Hoang, T. K. V., Ngoc Toan, V., Ngoc Toan, D., & Dang, L. H. (2019). Synthesis, biological evaluation and molecular docking study of 1,2,3-1H-triazoles having 4H-pyrano[2,3-d]pyrimidine as potential mycobacterium tuberculosis protein tyrosine phosphatase B inhibitors. *Bioorganic & Medicinal Chemistry Letters*, 29(2), 164–171. <https://doi.org/10.1016/j.bmcl.2018.12.009>
- Trott, O., & Olson, A. (2010). AutoDock Vina: Improving the speed and accuracy of docking with a new scoring function, efficient optimization, and multithreading. *Journal of Computational Chemistry*, 31(2), 455–461. doi: [10.1002/jcc.21334](https://doi.org/10.1002/jcc.21334).AutoDock.
- Verma, H., Choudhary, S., Kumar, M., & Silakari, O. (2021). In silico guided design of non-covalent inhibitors of DprE1: Synthesis and biological evaluation. *SAR and QSAR in Environmental Research*, 32(4), 333–352. <https://doi.org/10.1080/1062936X.2021.1900390>
- Wang, J., & Hou, T. (2012). Develop and test a solvent accessible surface area-based model in conformational entropy calculations. *Journal of Chemical Information and Modeling*, 52(5), 1199–1212. <https://doi.org/10.1021/ci300064d>
- Wang, Y., Sarris, K., Sauer, D. R., & Djuric, S. W. (2006). A simple and efficient one step synthesis of benzoxazoles and benzimidazoles from carboxylic acids. *Tetrahedron Letters*, 47(28), 4823–4826. <https://doi.org/10.1016/j.tetlet.2006.05.052>
- Warrier, T., Kapilashrami, K., Argyrou, A., Ioerger, T. R., Little, D., Murphy, K. C., Nandakumar, M., Park, S., Gold, B., Mi, J., Zhang, T., Meiler, E., Rees, M., Somersan-Karakaya, S., Porras-De Francisco, E., Martinez-Hoyos, M., Burns-Huang, K., Roberts, J., Ling, Y., ... Nathan, C. F. (2016). N-methylation of a bactericidal compound as a resistance mechanism in *Mycobacterium tuberculosis*. *Proceedings of the National Academy of Sciences of the United States of America*, 113(31), E4523–30. <https://doi.org/10.1073/pnas.1606590113>
- Yamashita, F. Y., & Hashida, M. H. (2004). In Silico Approaches for Predicting ADME Properties of Drugs. *Drug Metabolism and Pharmacokinetics*, 19(5), 327–338. <https://doi.org/10.2133/dmpk.19.327>
- Yuan, Y., Hu, Z., Bao, M., Sun, R., Long, X., Long, L., Li, J., Wu, C., & Bao, J. (2019). Screening of novel histone deacetylase 7 inhibitors through molecular docking followed by a combination of molecular dynamics simulations and ligand-based approach. *Journal of Biomolecular Structure & Dynamics*, 37(15), 4092–4103. <https://doi.org/10.1080/07391102.2018.1541141>